1 **Revision 2**

2

3 The Composition and Mineralogy of Rocky Exoplanets: A
4 Survey of >4,000 Stars from the Hypatia Catalog

5

6 Keith D. Putirka (kputirka@csufresno.edu) and John C. Rarick (jcrarick@outlook.com)
7 [1]Department of Earth and Environmental Sciences, Fresno State, 2345 E. San Ramon Ave,
8 MS/MH24, Fresno, CA 93720, 559-278-4524

9

10 **Abstract**

11 Combining occurrence rates of rocky exoplanets about Sun-like stars, with the number of such

12 stars that occupy possibly hospitable regions of the Milky Way, we estimate that at least 1.4 x

13 10^8 near-Earth-sized planets occupy habitable orbits about habitable stars. This number is highly

14 imprecise to be sure, and is likely much higher, but illustrates that such planets are common, not

15 rare. To test whether such rocky exoplanets might be geologically similar to Earth, we survey

16 >4,000 star compositions from the Hypatia Catalog—the most compositionally broad of such

17 collections. We find that rocky exoplanets will have silicate mantles dominated by olivine and/or

18 orthopyroxene, depending upon Fe partitioning during core formation. Some exoplanets may be

19 magnesiowüstite- or quartz-saturated, and we present a new classification scheme based on the

20 weight % ratio (FeO+MgO)/SiO$_2$, to differentiate rock types. But wholly exotic mineralogies

21 should be rare to absent; many exoplanets will have a peridotite mantle like Earth, but pyroxenite

22 planets should also be quite common. In addition, we find that half or more of the range of

23 exoplanet mantle mineralogy is possibly controlled by core formation, which we model using

24 $\alpha_{Fe} = Fe^{BSP}/Fe^{BP}$, where Fe^{BSP} is Fe in a Bulk Silicate Planet (bulk planet, minus core), on a

25 cation weight % basis (elemental weight proportions, absent anions) and Fe^{BP} is the cation

26 weight % of Fe for a Bulk Planet. This ratio expresses, in this case for Fe, the fraction of an

27 element that is partitioned into the silicate mantle relative to the total amount available upon

28 accretion. In our solar system, α_{Fe} varies from close to 0 (Mercury) to about 0.54 (Mars).

29 Remaining variations in theoretical exoplanet mantle mineralogy result from non-trivial

30 variations in star compositions. But we also find that Earth is decidedly non-solar (non-

31 chondritic); this is not a new result, but appears worth re-emphasizing, given that current

32 discussions often still use carbonaceous or enstatite chondrites as models of bulk Earth. While

33   some studies emphasize the close overlap of some isotope ratios between certain meteoritic and

34   terrestrial (Earth-derived) samples, we find that major oxides of chondritic meteorites do not

35   precisely explain bulk Earth. To allow Earth to be chondritic (or Solar), there is the possibility

36   that Earth contains a hidden component that, added to known reservoirs, would yield a

37   solar/chondritic bulk Earth. We test that idea using a mass balance of major oxides using known

38   reservoirs, so that the sum of upper mantle, metallic core and crust, plus a hidden component,

39   yields a solar bulk composition. In this approach, the fractions of crust and core are fixed and the

40   hidden mantle component, F_h, is some unknown fraction of the entire mantle (so if F_{DM} is the

41   fraction of depleted mantle, then $F_h + F_{DM} = 1$). Such mass balance shows that if a hidden mantle

42   component were to exist, it must comprise >28% of Earth's mantle, otherwise it would have

43   negative abundances of TiO_2 and Al_2O_3. There is no clear upper limit for such a component, so it

44   could comprise the entire mantle. But all estimates from $F_h = 0.28$ to $F_h = 1.0$ yield a hidden

45   fraction that does not match the inferred sources of ocean island or mid-ocean ridge basalts, and

46   would be geologically unusual, having higher Na_2O, Cr_2O_3 and FeO, and lower CaO, MgO and

47   Al_2O_3 compared to familiar mantle components. We conclude that such a hidden component

48   does not exist.

49

50   **Introduction**

51   Rapid and numerous discoveries of exoplanets have emerged in recent years, especially from

52   the Kepler (e.g., Thompson et al. 2018) and TESS missions (Vanderspek et al. 2018), which rely

53   on the dimming of light from an observed star, when a planet passes within line of sight,

54   providing a partial stellar eclipse. This transit method builds on other efforts that include radial-

55   velocity measurements, where orbiting planets exert gravitational tugs on stars, which then yield

56   measurable Doppler shifts in starlight (Cumming et al. 2008; Butler et al. 2017); microlensing

57   (e.g., Clanton and Gaudi 2014; Wambsganns 2016), where light from a more distant star is

58   gravitationally perturbed as it passes through an intervening planetary system; and direct imaging

59   (Janson et al. 2010; Clanton and Gaudi 2016; Baron et al. 2018). These measurements

60   demonstrate conclusively that exoplanets pervade the Milky Way.

61   Characteristics of known exoplanets are catalogued in the NASA exoplanet archive

62   (https://exoplanetarchive.ipac.caltech.edu/; n=3,917 as of this writing)—but the catalog is not

63   representative. Current detection methods, except perhaps microlensing (Wambsganns 2016), are

64   observationally biased towards large planets in small orbits (see Thompson et al 2018). In the

65   Kepler and TESS missions, for example, the transit of large planets yield a strong dimming

66   effect, and if they are in a tight orbit, then also more frequent (so reproduceable) signals. Perhaps

67   unsurprisingly, then, the median density of exoplanets in the NASA archive (n = 419, as density

68   is reported for only a small subset) is 0.98 g/cm^3 (compared to Earth's bulk density of 5.5 g/cm^3).

69   But this does not mean that Earth-sized planets with 1 A.U. orbits are uncommon. In an early

70   and controversial accounting of observational biases, Petigura et al. (2013) estimated that 11% of

71   Sun-sized stars in the Kepler database have near-Earth-sized planets that receive Earth-like

72   amounts of starlight. A new estimate by Mulders et al. (2018) increases that rate to 36%.

73   Occurrence rates for M-type stars (Dressing and Charbonneau 2013; 2015) are similar, although

74   habitable conditions there are less certain, as planets that orbit such cooler dwarf stars can be

75   tidally locked and exposed to frequent solar flares and intense UV radiation (see Dressing and

76   Charbonneau 2013). But even excluding M-dwarfs, the possible numbers of habitable, rocky

77   plants is vast. Ramirez et al. (2018) estimate that 4×10^8 Sun-like (F-, G- and K-type stars; the

78   Sun is G-type) occupy a galactic annulus of 7-9 kpc (kiloparsecs) from the Milky Way's center,

79   the Sun, being near the middle at 8 kpc. This region has been considered a galactic habitable

80   zone (Lineweaver et al. 2004), where stars have (a) sufficient metals to form planets (for

81   astronomers, a "metal" is any element heavier than He), and (b) limited exposure to lethal

82   radiation emanating from supernovae concentrated near the galactic core. Combined with the

83   Mulders et al. (2018) result, this annulus contains some 1.4×10^8 near-Earth-sized planets

84   occupying habitable orbits about habitable stars. The estimate is far from precise. For example,

85   Kraus et al. (2016) suggest that the dynamics of some binary star systems may preclude rocky

86   planet formation. But the value is probably a minimum. Recent studies (Prantzos 2006;

87   Gowanlock 2016; Kaib 2018) show that supernovae events are not as lethal as previously

88   thought and become rare with time (Gowanlock and Morrison 2018). In addition, while low

89   metallicity might yield fewer gas giants in the Milky Way's thick disk (e.g., Luck and Lambert

90   2011; Lemasle et al. 2013; Fischer and Valenti 2005), observations of rocky planets show no

91   impact of metallicity on their formation rate (Buchhave et al. 2012). Perhaps no part of the

92   galaxy is truly uninhabitable (e.g., Prantzos 2006; Kaib 2018). Finally, many argue (e.g.,

93   Dressing and Charbonneau 2013; Shields et al. 2016) that M-type stars may provide conditions

94   suitable for life, despite the above-noted challenges. Thus, while estimates for the number of

95 habitable, Earth-sized planets is imprecise, it is on the order of 10^8 or even 10^9, not 10^0 or 10^1;

96 they are numerous, not rare.

97 Recognition of this plethora of rocky, Earth-like planets has induced more than a little

98 curiosity about whether such exoplanets might exhibit plate tectonics (e.g., Weller and Lenardic

99 2018), and how geologic processes might be connected to the evolution of atmospheres, oceans,

100 and life (e.g., Stern 2006; Foley and Driscoll 2017). But this curiosity has not been matched by

101 knowledge of exoplanet compositional diversity. Are any exoplanets utterly exotic, made mostly

102 of oxides, or a strange mix of obscure silicates? Or are they mostly like Earth? And do

103 interstellar composition variations, or intra-planetary system processes exert hegemony over

104 rocky planet compositions? (We use "rocky" as an adjective to describe exoplanets, or other

105 planets in our inner solar system, that are like Earth; elsewhere, we use "terrestrial" to mean

106 rocks that are Earth-derived). Although knowledge of exoplanet compositions is scanty, some

107 recent studies have begun to fill the gap, applying Gibbs Free Energy Minimization models

108 (GFEMs) to predict silicate mantle mineralogies, for about a dozen planets (Unterborn et al.

109 2017; Hinkel and Unterborn 2018). But GFEMs are time-intensive and so not readily employed

110 to survey large numbers of compositions. And no GFEM has been tested to predict mineral

111 proportions in natural samples (e.g., see tests of our approach in Fig. 1). And to anticipate

112 another of our conclusions, GFEMs are based on experimental data that do not yet span the range

113 of MgO-poor, SiO_2-rich compositions (<20 wt. % and >50 wt. % respectively; Fig. 2b) that we

114 observe for some exoplanets; and so untested GFEMs (and our models also) require

115 extrapolation to obtain accurate mineral abundances.

116 To explore the compositional range of rocky exoplanets we examine star compositions from

117 the Hypatia Catalog (Hinkel et al. 2014; 2016). This catalog of nearby stars provides the broad

118 array of elemental compositions that are needed to test whether or not exoplanet compositions

119 are similar to Earth. Star compositions are derived from absorption spectra: a stellar interior

120 approximates a blackbody, and the radiated energy is partially absorbed as it passes through its

121 stellar photosphere. Absorption bands thus record the photosphere composition. Like other

122 studies (e.g., Tachinami et al. 2011; Duffy et al. 2015; Unterborn et al. 2017) we assume that this

123 photosphere approximates the composition of the proto-planetary disk from which planets

124 nucleate and grow. This assumption is founded upon the long-observed and stunningly close

125 match in composition between chondrite meteorites and the solar photosphere, for non-volatile

4

126   elements (Pottasch 1964; Ringwood 1966; Lodders and Fegley 2018). This match implies that

127   exoplanets should be similar in non-volatile composition to the stars they orbit. We test this

128   assumption by comparing the bulk compositions of Earth, Moon and Mars to the Solar

129   Photosphere. Our approach also allows us to evaluate a much greater fraction of stellar systems

130   in the Hypatia Catalog, yields a clearer analysis of error, and reveals voids in current data that

131   must be filled. We begin by comparing rocky exoplanet compositions to terrestrial rocks and

132   minerals; from these comparisons we derive a classification scheme that yields exoplanetary

133   mantle rock types from weight % ratios of $(FeO+MgO)/SiO_2$. We also use Thompson's (1982)

134   algebraic mass balance approach to recast major oxides into mineral proportions, with mineral

135   compositions derived from experimentally-equilibrated systems. As Thompson (1982) noted,

136   this approach can "save you time and money"—and so it does, allowing us to estimate mineral

137   proportions for thousands of bulk compositions, and to then plot our theoretical exoplanet

138   compositions using the classification schemes of Le Bas and Streckeisen (1991).

139   With this approach we examine >4,000 stars, or >80% of the Hypatia Catalog (Hinkel et al.

140   2014) to calculate theoretical exoplanet compositions. We assess how assumptions of planetary

141   temperature affect mineral proportions, which motivates our proposal of a "standard

142   mineralogy", as we discuss in the Methods section. We also test the effects of core formation,

143   taking Mercury, Earth and Mars as examples of mantle/bulk-planet Fe partitioning, which we

144   find to have a substantial effect on calculated mantle mineralogies.

145

146   **Methods**

147   **<u>General</u>**

148   We estimate the range of possible exoplanet compositions and mineralogies using 4,382 stars

149   from the Hypatia Catalog, taking all those entries where each of Na, Mg, Al, Si, Ca, Ti, Cr, Fe,

150   and Ni are reported. We choose the Hypatia Catalog for several reasons. First, it is the largest

151   catalog that examines nearby (within 150 pc) F-, G-, K-, and M-type (main-sequence, or H-

152   burning) stars; as previously noted, the Sun, is G-type (specifically G2V); the Milky Way is

153   roughly 25-30 kpc in diameter (Goodwin et al. 1998; Lopez-Corredoira et al. 2018). Second,

154   Hinkel et al.'s (2014) catalog reports a broader range of elements. Many stars only have reports

155   only of, say, Fe/H and/or Si/H; we require an array of elemental analyses to obtain more realistic

156   estimates of possible exoplanet mineralogy, and to test for the occurrence rate of mineralogical

5

157   oddities. Third, Hinkel et al. (2014) provide errors, or the "spread" of star compositions, which

158   they obtain by comparing multiple composition reports of a given star (see Hinkel et al. 2016).

159   This is important as we wish to propagate such uncertainties into errors on calculated exoplanet

160   mineralogy.

161   To obtain a Bulk Silicate Planet (BSP) composition (the bulk planet, minus its metallic core),

162   we assume that our hypothetical exoplanets have non-volatile element abundances that match the

163   stars they orbit. This assumption, fundamental to exoplanet studies (e.g., Tachinami et al. 2011;

164   Duffy et al. 2015; Unterborn and Panero 2017; Unterborn et al. 2017; Hinkel et al. 2018), stems

165   from a remarkable 1-to-1 correlation of non-volatile element abundances between the Sun's

166   photosphere and CI chondrite meteorites (e.g., Pottasch 1964; Ringwood 1966; Lodders and

167   Fegley 2018), and appears validated by a GFEM-approach of nebular condensation (Thiabaud et

168   al. 2015a). But as we will show, this assumption is imperfect.

169   Once we have a bulk planet (BP) composition, the silicate portion, BSP, is obtained by

170   subtracting a metallic core. To form a metallic core, we use the ratio $\alpha_{Fe} = Fe^{BSP}/Fe^{BP}$, where

171   Fe^{BSP} is Fe in a BSP, on a cation weight % basis (elemental weight proportions, absent anions)

172   and Fe^{BP} is the cation weight % of Fe for the Bulk Planet. Each of the planets Mercury, Earth and

173   Mars have proportionately different sized cores, and non-overlapping α_{Fe}, which we calculate

174   assuming either that $Fe^{BP} = Fe^{BSP} + Fe^{Core}$, or that $Fe^{BP} = Fe^{Solar}$, where Fe^{Solar} is also the cation

175   fraction of Fe, here on a non-volatile basis, and similar to the Fe cation fraction of carbonaceous

176   chondrites. As we detail below, we use Mercury, Earth and Mars as case studies: $\alpha_{Fe}^{Mercury} = 0.0\text{-}$

177   0.12; $\alpha_{Fe}^{Earth} = 0.263\text{-}0.494$; $\alpha_{Fe}^{Mars} = 0.54\text{-}0.58$. For Earth, we assume that the metallic core is 33%

178   by mass and has 5 wt. % Ni (Rubie et al. 2011), 2 wt. % S (Rubie et al. 2011; Wood et al. 2014)

179   and 4-7 wt. % Si (Wade and Wood 2005), leaving a core with 86-89 wt. % Fe. We use 87 wt. %

180   Fe in the core for all subsequent calculations. Rubie et al. (2011) also estimate that Earth's core

181   contains 0.5 wt. % O. But rather than model the uncertain behavior of O during core formation,

182   we instead employ α_{Fe}, as a combined proxy for oxygen fugacity (fO_2) and core formation

183   efficiency. As to BSP compositions, we also assume that whatever little C and S are retained

184   following accretion is segregated to near surface environments rather than retained in the mantle

185   (Fig. 2d). We test the fundamental assumption that stars provide an unfiltered view of exoplanet

186   compositions using the Sun (Lodders 2010) as input, to obtain a Solar Bulk Silicate Planet

187   composition, referred to as Sol-BSP. In principle, for some value of α_{Fe}, Sol-BSP should match

188   estimates of Bulk Silicate Earth (BSE; McDonough and Sun 1995; Salters and Stracke 2003;

189   Workman and Hart 2005; Palme and O'Neill 2014).

190

191   <u>Stellar Oxygen Abundances and Formation of a Metallic Core</u>

192   All Fe that is not partitioned into the core is treated as FeO total (FeOt). A critical question, is

193   whether exoplanets have sufficient O to oxidize all cations of interest, let alone Fe. Unterborn

194   and Panero (2017) find that if Earth is solar, O would be sufficiently abundant to oxidize all of

195   Earth's core. We obtain a similar result for theoretical exoplanets: of 3,266 stars in the Hypatia

196   Catalog where C, O, Mg, Si, and Fe are all reported, 97.8% have sufficient O to oxidize not just

197   all of Si, Mg and Fe (to SiO_2, MgO and FeO), but all available C to form CO_2. This is not to say

198   that O (or C) abundances are not important, and they are apparently challenging to measure in

199   stars (e.g., Ecuvillon et al. 2006), but mantle C-O abundances are affected by a myriad of

200   processes, including proto-planetary disk condensation (e.g., Thiabaud et al. 2015b; Unterborn

201   and Panero 2017), accretion (Rubie et al. 2015; Schaefer and Fegley 2017), and post-accretion

202   outgassing (Wade and Wood 2005; Schaefer and Fegley 2010); combining these to ascertain a

203   net planetary fO_2 is a fraught endeavor at best. Rather than estimate fO_2, our use of α_{Fe}, as

204   described above, serves as a combined proxy for fO_2 and core-formation efficiency, and obviates

205   the need for employing highly uncertain models.

206   Our use of α_{Fe} is specifically meant to examine how different scenarios of core formation

207   affect silicate mantle mineralogy. As in Unterborn et al. (2017), a fraction of bulk planetary Fe

208   (and Ni and Si) is removed to form the core, with the remainder staying in the mantle. This

209   process necessarily provisions the residual mantle with greater amounts of Si, Mg, and other

210   cations which, as we show, greatly impacts mantle mineralogy. As noted, for the ratio $\alpha_{Fe} =$

211   Fe^{BSP}/Fe^{BP}, the value of Fe^{BSP} is the cation weight % of Fe in a Bulk Silicate Planet (BSP),

212   relative to Fe^{BP}, the cation weight % of Fe for the bulk planet, core included, so $Fe^{BP} = Fe^{BSP} +$

213   Fe^{Core}. For Earth, we examine three cases. In two of these, we accept that total Fe in the mantle,

214   as FeO (FeOt, where "t" is "total") is 8 wt. % (McDonough and Sun 1995; Salters and Stracke

215   2003; Workman and Hart 2005; Palme and O'Neill 2014), which translates to $Fe^{BSP} = 11.3$ wt.

216   %, on a cation basis. If the bulk Earth has a solar bulk composition, $Fe^{BP} = 42.9$ wt. %, and α_{Fe}^{Earth}

217   is 0.263. If instead, we add to the mantle a core that is 33% Earth's mass and is 87 wt. % Fe, we

218   have $Fe^{BP} = 36.61\%$ and $\alpha_{Fe}^{Earth} = 0.311$. As a third case we assume that Earth's bulk mantle FeOt

7

219   is unknown, and subtract Earth's core (87 wt. % Fe, 33% Earth's mass) from a solar bulk

220   composition, which yields α_{Fe}^{Earth}= 0.494, and a mantle with 21.2 wt. % Fe (so about double the

221   estimates for BSE).

222   For the cases of Mars and Mercury, a solar bulk composition requires $\alpha_{Fe}^{Mars} = 0.537$ and

223    $\alpha_{Fe}^{Mercury} = 0.116$ to respectively obtain a martian mantle with 17.3 wt. % FeOt (Taylor 2013) and

224   a mercurian mantle with 3.5 wt. % FeOt (Morgan and Anders 1980). If we instead add a pure Fe

225   core (Rubie et al. 2015) of 22% planetary mass for Mars, and 68% planetary mass for Mercury,

226   to silicate mantles with 17.3% FeOt for Mars and 3.5wt. % FeOt for Mercury, we obtain $\alpha_{Fe}^{Mars} =$

227   0.58 and $\alpha_{Fe}^{Mercury} = 0.07$. But $\alpha_{Fe}^{Mercury}$ may be close to zero. Charlier et al. (2013) imply a nearly

228   FeOt-free mercurian mantle. Additionally, Keil (2010) suggests that the parent body of enstatite

229   achondrite (EA) meteorites is nearly Fe-free, and that the parent body might be Mercury. So we

230   use $\alpha_{Fe}^{Merc/EA} = 0$ as a possible end-member case for our solar system.

231   To complete the model of the core-formation process we add Ni and Si into the metallic cores

232   of theoretical exoplanets by applying an Earth-like $\alpha_{Ni} = Ni^{BSP}/Ni^{BP} = 0.08$ (where $Ni^{BSP} = 0.196$

233   wt. %, from McDonough and Sun, 1995; $Ni^{BP} = Ni^{Solar} = 2.54$ wt. %), and $Si^{BSP} = [1 -$

234    $C_{Si}^{Core}X^{core}]C_{Si}^{Stellar} = [1 - (0.07)(0.33)]C_{Si}^{Stellar} = [0.98]C_{Si}^{Stellar}$. Of course, light-alloying

235   element abundances in a metallic core might vary with planet size (Wade and Wood 2005), but

236   our results show that dissolving more or less Si (or Ni) into the core makes very little difference

237   to bulk mantle mineralogy.

238

239   <u>A Standard (Normative) Mineralogy & The Effects of Planetary Temperature</u>

240   As noted in the Introduction, we use the algebraic methods of Thompson (1982) to recast

241   oxide compositions into mineral proportions, which requires a choice of mineral compositions.

242   This choice should be viewed as a "standard", or normative mineralogy, as these terms were

243   used for terrestrial igneous rocks by Cross et al. (1902). A normative approach is useful here for

244   the very reasons that it was useful in the early 1900s. Calculated mineral norms were never

245   viewed as estimates of actual mineralogy, but instead allowed for discussions of compositional

246   contrasts in mineralogical terms. At that time, geologists knew quite little about the pressure-

247   temperature (*P-T*) conditions of igneous crystallization, or crystallization rates (*dT/dt*), but they

248   suspected that mineralogy depended upon these. Cross et al. (1902) thus proposed to calculate

249   the proportions of end-member mineral compositions, which they called "standard" or

8

250   "normative" minerals, which stood in contrast to the natural minerals, whose relative abundances

251   were called "modes".

252   For calculated exoplanet mineralogy, the problems are the same: exoplanetary T-fO_2

253   conditions (and P, for planets of varying size) are effectively completely unknown, and T and

254   fO_2 vary with time in any case, as planets cool and differentiate. Therefore, we estimate the

255   proportions of minerals using a "standard" mineralogy (see Fig. 3 caption), using mineral

256   compositions from the experiments of Walter (1998) and sub-solidus compositions used in

257   Putirka (2008). These compositions were selected so as to reproduce the bulk mineralogy of

258   depleted mantle (DM) of Workman and Hart (2005) when the Workman and Hart (2005) DM

259   bulk oxide composition is used as input. Our standard mineralogy approximates equilibrium at

260   1350°C at 2.0 GPa but can be found in experiments equilibrated from 1225-1450°C and 1-2.5

261   GPa. Our standard minerals thus also imply a standard set of P-T conditions. These conditions

262   are low enough to apply to any planet whose mantle reaches pressures of at least 2 GPa, which

263   will include any differentiated planet larger than Earth's Moon (whose core/mantle boundary is

264   at 5 GPa; for reference, Mercury's mantle reaches pressures of 8 GPa; Antonangeli et al. 2015).

265   We use such compositions, as opposed to idealized end-members, in the hope that our calculated

266   mineral proportions (Fig. 3) might approximate actual exoplanet mineralogies, and Fig. 1

267   provides some grounds for that aspiration: calculated fractions of olivine (Ol), orthopyroxene

268   (Opx) and clinopyroxene (Cpx) closely match measured mineral fractions in natural peridotites

269   (Warren 2016) and pyroxenites (Bodinier et al. 2009), at least when Cpx fractions are < 0.4 (the

270   case for all compositions we examine). Our tests imply that mineral modes are affected more by

271   bulk composition than solid solution. But Ol, Opx, and Cpx exhibit sufficient solid solution to

272   affect plotted mineral proportions in a Le Bas and Streckeisen (1991) diagram (Fig. 3). In that

273   figure we show arrows to indicate how compositions shift if one were to apply pure end-member

274   compositions, which are a proxy for a low temperature case of 800-950°C. We also use the noted

275   experiments to determine solid solution limits of Ol, Opx and Cpx, and so test whether

276   theoretical exoplanets are sufficiently rich in Al, Si or Ti to require saturation of phases such as

277   corundum, quartz or rutile, etc.

278   Results from GFEMs should be quite close to ours, and we do not suggest that GFEMs are

279   necessarily inaccurate; we only emphasize that they are an inefficient means to process

280   thousands of samples and have not been tested as in our Fig. 1. This study was inspired by

281   Robert Hazen's question about whether a planet's mineralogy is a function of chance or

282   necessity (Hazen et al. 2015); in all studies, including ours, the presumption is that at the very

283   high temperatures operating within a planetary interior that the laws of thermodynamics

284   necessitate a mineralogic outcome that hinges on bulk composition. There should be no intrinsic

285   bias to either method in that we expect the laws of thermodynamics to be the same, across time,

286   and across the Milky Way. But our experimental data are limited. A significant fraction of our

287   theoretical exoplanet BSPs (EBSPs) have simultaneously low MgO (<20wt. %) and high SiO_2 (>

288   50 wt. %), and these compositions fall outside the range of current experimental studies.

289   Experiments on these compositions may reveal new phases or even new solid solution limits, and

290   provide GFEMs with better control on the saturation of phases such as quartz, rutile or

291   corundum, etc.

292

293   Calculation Procedure: Converting Stellar Dex System Compositions to Silicate minerals

294   A theoretical exoplanetary silicate mantle composition and mineralogy is obtained as follows:

295   (1) Star compositions from the Hypatia Catalog (Hinkel et al. 2014), in dex-system notation, are

296   converted to weight % of elements (Supplementary Table 1) using the Solar Photosphere

297   composition of Lodders (2003, 2010). Total stellar Fe (which we take as Fe^{BP}) is multiplied by

298   Fe^{BSP}/Fe^{BP}, considering separate cases for Earth ($\alpha_{Fe}^{Earth} = 0.263\text{-}0.494$), Mercury ($\alpha_{Fe}^{Mercury} = 0.0\text{-}$

299   0.12), and Mars ($\alpha_{Fe}^{Mars} = 0.54\text{-}0.58$), to obtain estimates of Fe^{BSP}.

300   (2) Total Ni, or Ni^{BP}, is multiplied by $\alpha_{Ni} = 0.11$, and total Si, or Si^{BP}, is multiplied by $\alpha_{Si} = 0.93$

301   to obtain Ni^{BSP} and Si^{BSP} respectively (Supplementary Table 2).

302   (3) The entirety of Ti, Ca, Al, Cr, and Na are retained in the mantle, and we renormalize so that

303   $Ti + Ca + Al + Cr + Na + Fe^{BSP} + Ni^{BSP} + Si^{BSP} = 1$.

304   (4) Elemental abundances are converted to oxide weight %, with Fe calculated as FeOt.

305   (5) We apply the methods of Thompson (1982) to recast, for example, the oxides SiO_2, Al_2O_3,

306   FmO (FmO = FeO + MgO), and CaO, as proportions of Olivine (Ol) = Fm_2SiO_4, Orthopyroxene

307   (Opx) = $Fm_{1.9}Ca_{0.1}Al_{0.2}Si_{1.8}O_6$, Clinopyroxene (Cpx) = $Ca_{0.6}Fm_{1.4}Al_{0.2}Si_{1.8}O_6$ and Garnet =

308   $Fm_{2.7}Ca_{0.3}Al_2Si_3O_{12}$, where FmO = FeO+MgO (Supplementary Table 2). We also calculate

309   mineral proportions using pure minerals olivine (Fm_2SiO_4), clinopyroxene ($CaFmSi_2O_6$),

310   orthopyroxene ($Fm_2Si_2O_6$), and garnet ($Fm_3Al_2Si_3O_{12}$).

10

311   As we will show, most, but not all, possible exoplanets can be described as a positive

312   combination of Ol + Cpx + Opx + Gar. But we also examine minor phases, such as rutile (TiO_2),

313   chromite ($FeCr_2O_4$), corundum (Al_2O_3), quartz (SiO_2), albite ($NaAlSi_3O_8$), nepheline ($NaAlSiO_4$)

314   and bunsenite (NiO), to name a few, that might be globally saturated.

315

316   <u>Testing the Assumption that Stellar and Planetary Compositions are Identical</u>

317   As a test of our Methods, we treat the Sun as if it were just another star in the Hypatia

318   Catalog, deriving a BSP with a solar bulk composition (Sol-BSP). This is then compared to

319   estimates of Bulk Silicate Earth (BSE; McDonough and Sun 1995; Palme and O'Neill 2012;

320   Table 1) and depleted MORB-source mantle, DM (Salters and Stracke 2003; Workman and Hart

321   2005) (published estimates of DM and BSE are effectively identical). We also compare Bulk

322   Silicate Planet (BSP) estimates for Mars (see Taylor 2013) and Earth's Moon (see Kahn et al.

323   2006, and Longhi's 2006 LPUM) and we calculate a new BSE (Table 1) that accounts for a

324   compositionally distinct Plume Source Mantle (PSM) for ocean island and flood basalts that

325   appear to be a mixture of DM and subducted mid-ocean ridge basalt (MORB) (see Putirka et al.

326   2018 and references therein). For our new BSE, we assume that plumes tap some fraction, x, of

327   Earth's lower mantle, so that BSE = xPSM + (x-1)DM; Table 1 illustrates the case of x = 0.73,

328   where PSM constitutes the entirety of Earth's lower mantle.

329

330   **Results & Uncertainties**

331   <u>Exotic Mineralogies are Rare to Absent</u>

332   Among the >4,000 stars examined, we find that SiO_2, MgO, and FeO are the dominant oxides,

333   comprising ≥ 80% of all oxides for all stars examined. Like Hinkel and Unterborn (2018), we

334   find that the Sun is slightly enriched in Fe relative to the median of Hypatia stars (Fig. 2a) and

335   also has values close to the Hypatia median for other oxides (e.g., MgO, SiO_2 and Na_2O; Fig. 2).

336   But precise BSP compositions are sensitive to α_{Fe}. For example EBSPs in Fig. 2a, for the case of

337   α_{Fe} = 0.263, are shown as gray circles, whereas red circles show theoretical exoplanets when α_{Fe}

338   = 0.311; the latter have higher FeO by about 2 wt. %. For the case of α_{Fe} = 0.263, the range of

339   exoplanetary FeO in Fig. 2a implies silicate mantles that have 2-12 wt. % FeOt (median = 7.7 wt.

340   %), and metallic cores of pure Fe would vary proportionately in radius from -32% to +22%

341   relative to Earth (r_{median}^{core} = 3,421 km; r_{Earth}^{core} = 3,480 km).

11

342   Figure 2a also illustrates how assumptions of α_{Fe} affect estimates of Sol-BSP, which

343   represents the silicate mantle of a planet of Solar bulk composition: yellow symbols represent

344   calculations for the cases α_{Fe} = 0.263, 0.311 and 0.494. None of the estimates of Sol-BSP

345   intersect estimates of Bulk Silicate Earth (BSE; McDonough and Sun 1995; Palme and O'Neill

346   2012) or Depleted Mantle (DM, Salters and Stracke 2003; Workman and Hart 2005). Neither do

347   the Sol-BSP estimates match our new "BSE with PSM"; this estimate is derived using the plume

348   source composition from Putirka et al. (2011, 2018), where PSM = 20% Mid-Ocean Ridge

349   Basalt (MORB; Gale et al. 2013) plus 80% DM and assumes that PSM encompasses all of the

350   lower mantle (Fig. 2a). Even with such large amounts of PSM, this new estimate of BSE does

351   not reach the trend-line formed by the yellow symbols of Sol-BSP from various values of α_{Fe}. If

352   we instead assume that PSM only comprises the bottom-most portions of the lower mantle, then

353   "BSE with PSM" is driven away from MORB (black circle) and towards DM (blue circles), with

354   the result that "BSE with PSM" would then be little different from the BSEs of McDonough and

355   Sun (1995) and Palme and O'Neill (2012).

356   In Figure 2b, we compare theoretical exoplanets at α_{Fe} = 0.263 with terrestrial peridotites

357   (green circles) and pyroxenites (blue stars) (Fig. 2b; see caption for data sources). Exoplanets

358   clearly exhibit a wide range of MgO and SiO_2. At the high-MgO end of the peridotite array

359   (green circles, Fig. 2b) our terrestrial samples are dunites, and BSPs that range to greater MgO

360   are probably magnesiowüstite (Msw)-saturated. At the low-MgO/high SiO_2 end of the array (Fig.

361   2b), theoretical exoplanets range to higher SiO_2 than pyroxenites (blue stars, Fig. 2b), and

362   orthopyroxenes; since Opx has the highest Si content among common mantle phases, such

363   exoplanets may be saturated with quartz (Qtz). Aside from Msw and Qtz, it is not clear that

364   phases that are minor on Earth are dominant elsewhere. Clinopyroxene (Cpx) and garnet (Gar)

365   appear to exhibit sufficient solid solution capacity so as to absorb the small amounts of

366   exoplanetary Ca, Al and Ti, while olivine (Ol) can absorb Ni.

367   Sodium might be an exception, but the issue is unclear as Na is volatile (Palme 2000). In

368   Figure 2c, Na_2O in our calculated exoplanet BSPs are maxima, obtained by assuming no volatile

369   loss; for Sol-BSP, this amounts to 1.33-1.45 wt. % Na_2O. In contrast, BSE has just 0.13 – 0.36

370   wt. % Na_2O (Fig. 2b). Mars, also shown, has <40% of the Sol-BSP value (Taylor 2013). Since <

371   0.5% of theoretical exoplanets have >3.55 wt. % Na_2O (Fig. 2c), the vast majority of exoplanets

372   (99.5%) will have <0.9 wt. % Na_2O in their mantles if they retain Earth-like proportions of

12

373   Na_2O, and <1.3 wt. % Na_2O if they retain Mars-like proportions. Most of this Na can likely be

374   absorbed by pyroxene and garnet. For example, mean MORB has 2.79 wt. % Na_2O, and at high

375   pressures, this Na is absorbed by omphacite and garnet in eclogite. We thus suspect that minerals

376   such as albite are rare in exoplanetary mantles.

377

378   <u>Carbon and Sulfur; probably unimportant for mantle mineralogy</u>

379   In Fig. 2d, we calculate theoretical exoplanetary BSPs for all 2,543 stars in the Hypatia

380   Catalog where all our cations of interest (Na, Mg, Al, Si, Ca, Ti, Fe) and each of C and S are

381   reported, with C treated as CO_2 (Supplementary Table 3). To these we compare estimates of

382   Earth's mantle (McDonough and Sun 1995; Salters and Stracke 2003), Bulk Silicate Mars

383   (Morgan and Anders 1979; Lodders and Fegley 1997), average CI chondrites (McDonough and

384   Sun 1995), and Sol-BSP. All BSPs are calculated for the highly idealized case that all S and C

385   are retained by a planet, and that neither enter the core. These assumptions are, of course,

386   unrealistic, but provide ball-park depletion factors due to a combination of nebular condensation,

387   accretion, core formation and mantle devolatilization processes: in this idealized case, Earth's

388   mantle has retained <0.7% S and <0.006% of CO_2 relative to the idealized Sol-BSP case. This is

389   not to say that C and S contents are uninteresting. Carbon is clearly essential for life and its

390   global cycle may affect climate (Sleep and Zahnle 2001). But absent new high *P-T* experiments

391   that indicate the existence of refractory S- and C-rich phases, neither element appears crucial for

392   understanding the dynamics of planetary interiors.

393

394   <u>Earth is Non-Solar (and Non-Chondritic)</u>

395   We also find that Sol-BSP does not match published estimates of BSE. This means either (a)

396   that published estimates of Bulk Silicate Earth (BSE) are in error or (b), a fundamental

397   assumption in exoplanet composition studies is wrong: exoplanets do not precisely mimic the

398   stars they orbit. To be clear, we are not certain which of (a) or (b) is the actual case, but there is a

399   definite choice that must be made. Nickel provides a minor but perhaps significant example: a

400   Solar bulk Earth (2.54 wt. % Ni) and a mantle with 0.196 wt. % Ni (McDonough and Sun 1995)

401   yields $\alpha_{Ni}^{Earth} = 0.08$, but this requires a core with 7.3% Ni, greater than the 5% Ni usually

402   inferred (e.g., Wood et al. 2014). Perhaps terrestrial Ni contents are uncertain, but Fe is more

403   problematic. By design, applying $\alpha_{Fe}^{Earth} = 0.263$ yields a Sol-BSP with a BSE-like FeOt of 8 wt.

13

404   %, and this yields a pure-Fe core radius, $r_{Sol-BSP}^{core}$ of 3,483 km, assuming mean core density is

405   11,247 kg/km^3 (from the Preliminary Reference Earth Model or PREM; Anderson 1989)—

406   stunningly and deceivingly close to Earth's 3,480 km. But SiO$_2$ for the resulting Sol-BSP is high,

407   at 48.4% (or 48.9% if we add no Si to the core), compared to 45% for BSE—a difference that is

408   not trivial from a mineralogical perspective. And of course, Earth's core is not pure Fe, but

409   instead has 85-89% Fe (Rubie et al. 2011; Wood et al. 2014). If we maintain $\alpha_{Fe}^{Earth} = 0.263$, no

410   reasonable amount of Si in the core brings SiO$_2$ contents into agreement. If we instead obtain

411   Fe^{BSP} by subtracting Earth's core (assuming it is 87% Fe), then $\alpha_{Fe}^{Earth} = 0.494$, and Sol-BSP has

412   a BSE-like SiO$_2$ (44.9 wt. %), but much greater FeOt (15.6 wt. %; Fig. 2a) and lower MgO

413   (30.8% vs. BSE's ca. 38-39%; Table 1). To yield a Sol-BSP with 8 wt. % FeOt at $\alpha_{Fe}^{Earth} = 0.494$,

414   Earth's core would have to be >40% of Earth's mass, instead of the observed 33%. In summary,

415   no value of α_{Fe}^{Earth} yields a Sol-BSP that simultaneously matches BSE's SiO$_2$, MgO, and FeOt

416   (Fig. 2a); and hence the trend of Sol-BSP estimates obtained using different α_{Fe}^{Earth} values do

417   not intersect BSEs in Fig. 2.

418

419   <u>Hypothetical Exoplanet Mineralogy, and Temperature-derived Uncertainty</u>

420   Figure 3 shows that while most hypothetical exoplanets plot as peridotites or pyroxenites, the

421   dominant variation in calculated exoplanet mineralogy involves a tradeoff between Ol and Opx;

422   variations in Cpx (and garnet, not shown) are small in comparison, because across the Hypatia

423   Catalog, the ranges of CaO and Al$_2$O$_3$ are small compared to ranges in SiO$_2$, FeO and MgO.

424   Figure 3 also shows how mineralogy varies as a function of α_{Fe}. We anticipate that exoplanetary

425   systems will likely have planets that exhibit a range of mineralogies (even for a given Mg/Si),

426   just as α_{Fe} varies within our solar system. To illustrate the magnitude of the effect of α_{Fe}, we

427   plot median exoplanet mineralogies as large black crosses in Fig. 3: for $\alpha_{Fe} = 0.263$, median

428   exoplanets have 38% Ol. But for a Mars-like α_{Fe} 0.537, median Ol rises to 60%, and for a

429   Mercury-like $\alpha_{Fe} = 0.0$, mean Ol drops to 19%. This shift is directly related to how Fe is

430   partitioned between core and mantle: adding Fe from the core to the mantle (higher α_{Fe})

431   increases (FeO+MgO)/SiO$_2$ and effectively dilutes Si in the mantle, which increases Ol content;

432   in contrast, placing more Fe into the metallic core reduces (FeO+MgO)/SiO$_2$ and SiO$_2$ is

433   enriched in the residual mantle, which increases Opx. We also find that an assumed planetary

434   temperature (T) affects mineral proportions (Fig. 3). All of the plotted compositions in Fig. 3

435   assume a high-T case (1350°C; see Methods) where minerals exhibit extensive solid solution. At

436   low T (<950°C), solid solution would decrease; the black arrows in Fig. 3c illustrate the strong

437   shift towards Ol with lesser degrees of solid solution. To understand why, consider that Fig. 3

438   effectively illustrates a competition between MgO- (Ol), SiO$_2$- (Opx) and CaO-rich (Cpx)

439   phases. At low T, Opx dissolves less Al and more Si into its tetrahedral site (as does Cpx), and so

440   at low-T, less Opx is needed to accommodate the same amount of SiO$_2$ in a given bulk

441   composition, so a system shifts towards the Ol apex. With smaller total amounts of SiO$_2$ in a

442   bulk composition (compositions that are already near the Ol apex) the magnitude of the shift is

443   less. Shifts toward or away from Cpx are subdued and affected by renormalization in the

444   projection from garnet; this is because total Cpx is controlled by Ca, which is a minor component

445   in planetary bulk compositions; in isolation, higher Ca (i.e., lower T) in Cpx shifts mineral

446   proportions away from the Cpx apex. Interstellar variations in Ca and Al provide minor shifts in

447   normative Cpx and Gar abundances, but these elements are too low in total abundance to require

448   other Ca- or Al-rich phases.

449

450   <u>Other Sources of Variability and Uncertainty</u>

451   A source of uncertainty arises from the "spread" in published stellar compositions (Hinkel et

452   al. 2014), which represent the range of reported values of elemental concentrations. When

453   translated to mineral proportions, the magnitude of the "spread" translates to slightly less than

454   the size of the large circles (for Sol-BSP and BSE) in Fig. 3. Current experiments, and our tests

455   of mineral fraction estimates (Fig 1) use bulk compositions that mostly range from 40-49 wt. %

456   SiO$_2$, and 20-50 wt. % MgO, but many EBSPs fall outside these ranges; new experiments may

457   reveal unique mineral assemblages that are not extant among terrestrial mantle samples.

458

459   **Discussion**

460   <u>An Exoplanet Classification Model & Sources of Uncertainty</u>

461   However imperfect our mineral estimation methods might be, we can be certain from the

462   Hypatia Catalog (Hinkel et al. 2014) that many if not most exoplanets will have silicate mantles

463   that mimic lithologies found on Earth (Figs. 2a, b), and that either or both of Ol and Opx will be

464   dominant (Fig. 3). Some planets may approach monomineralic dunite or orthopyroxenite, and

15

465   some may have sufficient MgO so as to be magnesiowüstite (Msw)-saturated (Fig. 2b), or

466   sufficient SiO_2 to be saturated in quartz (Table 2). But none of our hypothetical exoplanets

467   appear wholly exotic (i.e., have mantles made of rutile or corundum or albite, etc.), and even

468   inter-stellar variations in Cpx (Fig. 3) and garnet are quite narrow.

469   Figure 4 illustrates our proposed classification scheme based on the ratio (FeO+MgO)/SiO_2

470   for a given Bulk Silicate Planet (BSP) composition (Table 2; Fig. 4). This approach does not

471   yield mineral proportions but separates observable rock types (peridotites and pyroxenites) and

472   solid solution limits of olivine and orthopyroxene. Such estimates of mantle rock type, however,

473   are very sensitive to assumed values of α_{Fe}: as α_{Fe}, varies from 0 to 0.537 (Fig. 3) mean

474   exoplanetary Ol contents shift from about 20% to 60% Ol (Fig. 3), and mantle rock types shift

475   from 59% pyroxenite to 95% peridotite (Table 2). In addition, planets do not necessarily

476   compositionally mimic the stars they orbit; Mars is plausibly solar in bulk composition (Figs. 4d-

477   f) but Earth is non-solar (Figs. 2-3; Figs. 4a-c). And predicting how exoplanets might deviate

478   from a stellar composition might not be straightforward. For example, Palme (2000) suggests

479   that no compositional gradients exist from Mercury to Vesta, and we find the same: α_{Fe} increases

480   from near 0 to 0.54 from Mercury to Mars, but $\alpha_{Fe} = 0.13$ at Vesta, using Steenstra et al. (2016).

481   So planet-star distance might not be helpful in narrowing an exoplanetary bulk composition.

482

483   <u>Peridotite vs. Pyroxenite? The Difference Might be Important</u>

484   Seemingly subtle differences in mantle mineralogy may be important. Compared to a

485   peridotite planet, a pyroxenite planet may yield thicker crust (Lambart et al. 2016), albeit still

486   basaltic in composition (Lambart et al. 2009). It is not clear what effect this might have on plate

487   tectonics. A thick, rigid, Opx-rich crust might be stronger (e.g, Yamamoto et al. 2008), and less

488   likely to break into plates. Alternatively, with sufficient water, Opx-rich systems might partially

489   distill into very thick silicic crustal bodies, and so enhance crustal and lithosphere density

490   contrasts. New experiments are needed on the melting and yield strength behaviors of MgO- and

491   Opx-rich compositions (Supplementary Tables 2-3) to understand these systems.

492

493   <u>Earth is Non-Solar/Non-Chondritic</u>

494   We verify a long-standing result: Earth's bulk composition is non-solar and non-chondritic

495   (e.g., McDonough and Sun 1995; Drake and Righter, 2002). The problem of a Solar bulk Earth

16

496   with respect to the non-volatile elements is encapsulated by the tradeoff in predicting SiO_2 or

497   FeO: if $\alpha_{Fe}^{Earth} = 0.263$ (a solar bulk composition and a BSE with 8 wt. % FeO), then Earth's

498   mantle has less SiO_2 than carbonaceous chondrites which, as expected, are similar to Sol-BSP

499   (Figs. 2a, 5b). And the mis-match in SiO_2 is worse still for enstatite chondrites (Fig. 5a-c). But if

500   we apply $\alpha_{Fe} = 0.494$ (a solar bulk Earth with a core having 87% Fe and unknown mantle FeO

501   content), this yields a BSE-like SiO_2 (Fig. 2a, 5e), but FeO contents much higher than anything

502   presumed for BSE (Figs. 2a, 5e). If we instead allow that Si has been lost to an early atmosphere

503   (Fegley et al. 2016) or to the core (Wade and Wood 2005), Earth still has higher-than-solar CaO

504   and Al_2O_3 (Fig. 5c). The contrasts in SiO_2 may seem minor, but they make a tremendous

505   difference in mantle mineralogy: at $\alpha_{Fe}^{Earth} = 0.263$, Sol-BSP plots solidly in the pyroxenite field

506   and at $\alpha_{Fe}^{Earth} = 0.494$ it is still Ol-poor compared to BSE (Fig. 3). These results might appear to

507   bolster arguments for a pyroxenite-rich mantle, derived by adding subducted mid-ocean ridge

508   basalt (MORB) to depleted mantle (e.g., Hirschmann and Stolper 1996; Sobolev et al. 2007; van

509   der Hilst and Karason 2000). But if the true BSE is obtained by adding MORB, then BSE moves

510   further from Sol-BSP with respect to FeOt (Fig. 2a), CaO and Al_2O_3 (Fig. 5c).

511

512   <u>Does Earth Have a Hidden Mantle Component or a Compositionally Distinct Lower Mantle?</u>

513   A remaining and alluring alternative to obtain a solar or chondritic bulk Earth is to assume

514   that Earth's mantle contains a hidden component, *h*. Seismological arguments have long been

515   advanced to yield a lower mantle that is enriched in FeO (e.g., Anderson and Jordan 1970; van

516   der Hilst and Karason 2000), or SiO_2 (e.g., Murakami et al. 2012), although these perennially fail

517   re-inspection (e.g., Davies, 1974; Irfune et al. 2010; Davies et al. 2012; Hyung et al. 2016). In

518   any case, Agee and Walker (1988) posit a viable mechanism: high-pressure phases, such as

519   bridgmanite or majorite (both nominally $(Mg,Fe)SiO_3$ but dissolving variable Ca, Al and other

520   cations) might crystallize from an ancient magma ocean and settle into the lower mantle. The

521   possibility of a hidden component, un-excavated by mantle plumes, has also gained support from

522   isotopic studies that show that terrestrial samples are not chondritic, but where the whole Earth is

523   assumed to be so (Boyet and Carlson 2005; Bouvier and Boyet 2016). Figure 5 shows that

524   adding near-equal amounts of bridgmanite and majorite to BSE could yield Solar-like MgO and

525   SiO_2 (Fig. 5a); such additions might yield too low a value of FeO (Fig. 5b), but the mineralogy

17

526   of the deep mantle is not well known, and other phases might compensate, so the idea of Agee

527   and Walker (1988) is possible.

528   As a further test, we delimit the major oxide compositional range of h (Table 2) by subtracting

529   from a solar bulk composition (a) Earth's core (assuming 87 wt. % Fe), and (b) the depleted

530   mantle (DM) component that is needed to feed mid-ocean ridge basalts. In this model, the

531   fraction of the hidden component, F_h and the fraction of DM, F_{DM} are both unknown, but they

532   sum to unity (note that continental crust is too low in abundance to affect major oxide mass

533   balance), and the sum is equivalent to bulk silicate Earth at $\alpha_{Fe} = 0.494$: so $F_h + F_{DM} = 1 = $ Sol-

534   BSP($\alpha_{Fe} = 0.494$). This mass balance test shows that h must be >28% of Earth's mantle,

535   otherwise Al_2O_3 and TiO_2 in h are negative (Table 1); this fraction is much greater than the <3%

536   volume estimated for seismic anomalies hypothesized to represent a hidden component (see He

537   and Wen 2012). It would represent everything below about 1,850 km, and so approximate the

538   bottom 1,000 km of the mantle (e.g., Albarede and van der Hilst 2002), but this component

539   would be effectively Ca- and Al-free. For the case where $F_h = 0.73$ (where F_h is all of Earth's

540   lower mantle) no composition of h yields a plume source mantle (PSM; Table 1) that would feed

541   ocean island basalts (Table 1), as FeO contents are too high and CaO and Al_2O_3 contents are too

542   low (Table 1). If we adopt Javoy et al.'s (2010) enstatite chondrite bulk Earth (Javoy et al. 2010)

543   we obtain a lower mantle that is much less extreme in its Fe-enrichment (9.24 wt. % FeO), but

544   SiO_2 is quite high (51.5 wt. %), and MgO is low (35.2 wt. %), as are CaO (1.4 wt. %) and Al_2O_3

545   (1.8 wt. %), especially relative to PSM.

546   In summary, if h exists, it is not only quite large, but it is *not* the source of mantle plumes

547   (PSM in Table 2) and it is enriched in Na_2O and FeO, and depleted in MgO, CaO and Al_2O_3,

548   compared to any estimates of BSE or DM. Our conclusion is to reject h since to accept it requires

549   rejecting long-standing arguments in support of whole-mantle convection (e.g., Davies, 1977),

550   the nucleation of thermal plumes near the core/mantle boundary (Davies 1988; Davies and

551   Richards 1992), and thermal models (Farnetani 1997) that explain observed plume excess

552   temperatures (Putirka 2005; Putirka et al. 2007). Especially compelling are seismic images of

553   subducted slabs that reach the base of the mantle (Jordan 1977; Grand 1997; Fukao and

554   Obayashi 2013); these require a return flow and appear to end discussion of an isolated lower

555   mantle. Numerical models also appear to resolve supposed conflicts between whole-mantle

556   convection and a mantle with geochemical and seismic heterogeneity (Jordan et al. 1993;

18

557 Schuberth et al. 2009; Barry et al. 2018). So while controversy still exists over seismic images of

558 deep-seated plumes (e.g., Montelli et al. 2004), we agree with the recent work of Agrusta et al.

559 (2018), that Earth's mantle has long been well stirred. But if all these studies are in error, Table 2

560 provides estimates for lower mantle composition, for three cases: that h exists below 1,850 km (a

561 minimum volume), 1,000 km and 660 km.

562
563 **Implications**
564

565   A key implication is that Table 2 can be used to better interpret bulk densities of rocky

566 exoplanets. For example, there has been much interest in the TRAPPIST-1 system because there,

567 seven rocky, more-or-less Earth-sized, exoplanets have been discovered (Gillon et al. 2017).

568 Several studies have thus ensued, attempting to narrow their bulk densities (see Quarles et al.

569 2017; Rackham et al. 2018; Grimm et al. 2018; Unterborn et al. 2018; values range from 3.3 to

570 6.5 g/cm^3 in the NASA exoplanet archive). If core size can be determined (e.g, Zeng et al. 2016),

571 then host star composition, Table 2, and the spread of planetary compositions in our own solar

572 system (Fig. 4), should delimit the range of exoplanet bulk silicate mineralogy in the

573 TRAPPIST-1 or any other system. The soon-to-be-launched James Webb Space Telescope

574 (JWST) will also measure exoplanetary atmospheres (e.g., Beichman et al. 2014), and possible

575 biogenic signatures (Krissansen-Totton et al. 2018)—our work provides insights to the geology

576 beneath such atmospheres and might even be testable from certain JWST observations (e.g,

577 Bodman et al. 2018).

578   We also find that although theoretical exoplanet mineralogy can vary widely, that variation is

579 restricted to a near-linear array, involving orthopyroxenite (possibly quartz-bearing) and dunite

580 (possibly magnesiowüstite-bearing) (Fig. 3). Such results indicate no obvious barrier to the

581 evolution of exoplanetary felsic (continental) crust, or plate tectonics. Metallic cores may be

582 proportionately smaller or larger than Earth's, but for Earth-sized planets, no mantle depths

583 would be too shallow to limit mantle convection. And if Opx and Ol have similar high-

584 temperature viscosities (Bystricky et al. 2016) mantle convection would also not vary with bulk

585 composition (note that radioactive elements appear to be sufficiently abundant to allow a long-

586 lived convecting interior on most exoplanets; Unterborn et al. 2015). However, if Opx has a

587 greater viscosity than Ol at low temperatures (e.g., Yamamoto et al. 2008; Bystricky et al. 2016)

588 then pyroxenite planets might have stronger lithosphere, and so resist tectonic deformation

19

589   (Weller and Lenardic 2018), although current experiments leave the viscosity contrast uncertain

590   (see Hansen and Warren 2015). On the other hand, pyroxenite planets might have thicker and

591   more abundant basaltic crust (Lambart et al. 2009, 2016), which might then distill into SiO_2-rich

592   (granitic) crust (e.g., Sisson et al. 2005), which could then heighten lithospheric density contrasts

593   and enhance tectonic initiation. New experiments are desperately needed.

594   Finally, efforts to use chondrites as a possible bulk composition for Earth (e.g., Boyet and

595   Carlson 2005; Fitoussi et al. 2009; Javoy et al. 2010) appear misguided. We agree with

596   McDonough and Sun (1995) that chondrite meteorites "are not the main building blocks of

597   Earth". Our major oxide comparisons (Fig. 5) support the conclusion of Drake and Righter

598   (2005), that our planet is constructed of "Earth Chondrites". Estimates of Bulk Silicate Earth

599   SiO_2-MgO-FeO plot at the edge of or outside the array of carbonaceous and enstatite chondrite

600   meteorites (Fig. 5). The lack of chondrites in the vicinity of BSE may mean that the

601   planetesimals that formed Earth were consumed during Earth's accretion (e.g., the "Earth

602   Chondrites" of Drake and Righter 2005). This does not mean that planets never match the

603   composition of the stars they orbit. Mars is plausibly solar (or carbonaceous chondritic) in bulk

604   composition (Figs. 5d-f). But perhaps chondrites have always been a red herring. Hewins and

605   Herzberg (1996) proposed that chondrules might be an important component in Earth. Iron

606   contents seem too low for chondrules to comprise bulk Earth, but the match to silicate Earth is

607   close for chondrule-rich meteorites, and Connolly and Jones (2016) suggest that they are among

608   the most abundant components of the early Solar System. In sum, to better understand

609   exoplanets, we need to dispel the shadow that is cast over current knowledge of our own early

610   Solar System.

611

612

613   **Acknowledgments**

623   Alain Plattner and John Wakabayashi provided very helpful comments on early drafts of this
624   manuscript; Plattner's questions in particular prompted our investigation of a_{Fe}. We especially
625   thank Natalie Hinkel for answering our many questions about the Hypatia Catalog, to Cayman
626   Unterborn for sharing a version of his spreadsheet for transforming stellar compositions from
627   dex to major oxides, and to both Natalie and Cayman for sharing pre-prints of their work, and
628   explaining ideas and methods expressed in these.

629

630   **References Cited**
631   Agee, C.B., and Walker, D. (1988) Mass balance and phase density constraints on early
632   differentiation of chondritic mantle. Earth and Planetary Science Letters, 90, 144-156.
633   Agrusta, R., van Hunen, J. and Goes, S. (2018) Strong plate enhance mantle mixing in early
634   Earth. Nature Communications, 9, 1-10, doi: 10.1038/s41467-018-05194-5.
635   Albarede, F., and van der Hilst, R.D. (2002) Zoned mantle convection. Philosophical
636   Transactions: Mathematical, Physical and Engineering Sciences, 360, 2569-2592.
637   Anderson, D.L. (1989) Theory of Earth. Blackwell Scientific Publications, Brookline Village,
638   MA, 366 p.
639   Anderson, D.L. and Jordan, T. (1970) The composition of the lower mantle. Physics of Earth and
640   Planetary Interiors, 3, 23-35
641   Antonangeli, D., Morard, G., Schmerr, N.C., Kombayashi, T., Krisch, M., Fiquet, G., and Fei, Y.
642   (2015) Toward a mineral physics reference model for the Moon's core. Proceedings of the
643   National Saacdemy of Sciences, U.S.A., 112, 3916-3919.
644   Baron, F. et al. (2018) WEIRD: Wide-orbit exoplanet search with infrared direct imaging. The
645   Astronomical Journal, 156:137, 19 pp.
646   Barry, T.L. Davies, J.H., Wolstencroft, M., Millar, I.L., Zhao, Z., Jian, P. Safovana, I., and Price,
647   M. (2018) Whole-mantle convection with tectonic plates preserves long-term global patters of
648   upper mantle geochemistry. Scientific Reports, 7, doi: 10.1038/s41598-017-01816-y
649   Beichman, C., et al. (2014) Observations of transiting exoplanets with the James Webb Space
650   Telescope. Publications of the Astronomical Society of the Pacific, 126, 1134-1173.
651   Bodinier, J-L., Garrido, C.J., Chanefo, I., Bruguier, O., and Gervilla, F. (2008) Origin of
652   pyroxenite-peridotite veined mantle by refertilization reactions: evidence from the Ronda
653   Peridotite (southern Spain). Journal of Petrology, 49, 999-1025.
654   Bodman, E.H.L., Wright, J.T., Desch, S.J., and Lisse, C.M. (2018) Inferring the composition of
655   disintegrating planet interiors from dust tails with future James Webb pace Telescope
656   Observations. The Astronomical Journal, 156:117, 8 pp.
657   Bouvier, A., and Boyet, M. (2016) Primitive solar system materials and Earth share a common
658   initial [142]Nd abundance. Nature, 537, 399-402.
659   Boyet, M., and Carlson, R.W. (2005) [142]Nd evidence for early (>4.53 Ga) global differentiation
660   of the silicate Earth. Science, 309, 576-581.
661   Buchhave, L.A., et al. (2012) An abundance of small exoplanets around stars with a wide range
662   of metallicities. Nature, 486, 375-377.
663   Butler, R.P., et al. (2017) The LCES HIRES/Keck precision radial velocity exoplanet survey.
664   The Astronomical Journal, 153:208, 19 pp.
665   Bystricky, M., Lawlis, J., Mackwell, S., Heidelbach, F., and Raterson, P. (2016) High-
666   temperature deformation of enstatite aggregates. Journal of Geophysical Research, doi:
667   10.1002/2016JB13011.

668 Campbell, I.E., and Taylor, S.R. (1983) No water, no granites – no oceans, no continents.
669   Geophysical Research Letters, 10, 1061-1064.
670 Charlier, B., Grove, T.L., and Zuber, M.T. (2013) Phase equilibria of ultramafic compositions on
671   Mercury and the origin of the compositional dichotomy. Earth and Planetary Science Letters,
672   363, 50-60.
673 Chayes, F. (1960) On correlation between variables of constant sum. Journal of Geophysical
674   Research, 65, 4185-4193.
675 Clanton, C. and Gaudi, B.S. (2014) Synthesizing exoplanet demographics from radial velocity
676   and microlensing surveys. II. The frequency of planets orbiting dwarfs. The Astrophysical
677   Journal, 791:91, 23 pp.
678 Clanton, C. and Gaudi, B.S. (2014) Synthesizing exoplanet demographics: a single population of
679   long-period planetary companions to M dwarfs consistent with microlensing, radial velocity,
680   and direct imaging surveys. The Astrophysical Journal, 819:125, 42 pp.
681 Connolly, H. Jr., and Jones, R. () Chondrules: the canonical and non-canonical view. Journal of
682   Geophysical Research, 10.1002/2016JE005113.
683 Cross, W., Iddings, J.P., Pirsson, L.V., and Washington, H.S. (1902) A quantitative chemico-
684   mineralogical classification and nomenclature of igneous rocks. Journal of Geology, 10, 555-
685   690.
686 Cumming, A., Butler, R.P., Marcy, G.W., Vogt, S.S., Wright, J.T., and Fischer, D.A. (2008) The
687   Keck planet search: detectability and the minimum mass and orbital period distribution of
688   extrasolar planets. Publications of the Astronomical Society of the Pacific, 120, 531-554.
689 Daly RA. (1946) Origin of the Moon and its topography. Proceedings of the American
690   Philosophical Society, 90, 104–119.
691 Davies, G.F. (1974) Limits on the constitution of the lower mantle. Geophysical Journal of the
692   Astronomical Society, 38, 479-503.
693 Davies, G.F. (1977) Whole-mantle convection and plate tectonics. Geophysical Journal of the
694   Royal Astronomical Society, 49, 459-486.
695 Davies, G.F. (1988) Ocean bathymetry and mantle convection 1. Large-scale flow and hotspots.
696   Journal of Geophysical Research, 93, 10467-10480.
697 Davies, D.R., Goes, S., Davies, J.H., Schuberth, B.S.A., Bunge, H.-P., and Ritsema, J. (2012)
698   Reconciling dynamic and seismic models of Earth's lower mantle: the dominant role of
699   thermal heterogeneity. Earth and Planetary Science Letters, 353-354, 253-269.
700 Davies, G.F. and Richards, M.A. (1992) Mantle convection. Journal of Geology, 100, 151-206.
701 Drake, M.J. and Righter, K. (2002) Determining the composition of the Earth. Nature, 416, 39-
702   44.
703 Dressing, C.D. and Charbonneau, D. (2013) The occurrence rate of small planets around small
704   stars. Astrophysical Journal, 767, arXiv:1302.1647.
705 Dressing, C.D. and Charbonneau, D. (2015) The occurrence of potentially habitable planets
706   orbiting M dwarfs estimated from the full Kepler dataset and an empirical measurements of
707   detection sensitivity. Astrophysical Journal, 807, doi:10.88/0004-637X/807/1/45.
708 Duffy, T., Madhusudhan, N., and Lee, K.K.M. (2015) Mineralogy of super-Earth planets.
709   Treatise on Geophysics, 2nd Ed., 2, 149-178.
710 Ecuvillon, A., Israelian, G., Santos, N.C., Schukina, N.G., Mayor, M., and Rebolo, R. (2006)
711   Oxygen abundances in planet-harbouring stars. Astronomy and Astrophysics, 445, 633-645.
712 Farnetani, C.G. (1997) Excess temperature of mantle plumes: the role of chemical stratification
713   across D". Geophysical Research Letters, 24, 1583-1586.

22

714   Fegley Jr., B., Jacobson, N.S., Williamns, K.B., Plane, J.M.C., Schefer, L., and Lodders, K.
715   (2016) Solubility of rock in steam atmosphere of planets. The Astrophysical Journal, 824:103.
716   Fischer, D.A. and Valenti, J. (2005) The planet-metallicity correlation. The Astrophysical
717   Journal, 622, 1102-1117.
718   Fitoussi, C., Bourdon, B., Keline, T., Oberli, F., and Reynolds, B.C. (2009) Si isotope
719   systematics of meteorites and terrestrial peridotites: implications for Mg/Si fractionation in
720   the solar nebula and for Si in the Earth's core. Earth and Planetary Science Letters, 287, 77-
721   85.
722   Foley, B.J. and Driscoll, P.E. (2017) Whole planet coupling between climate, mantle, and core:
723   implications for the evolution of rocky planets. arXiv:1711.06801v1 [astro-ph.EP] 18 Nov
724   2017.
725   Fukao, Y. and Obayashi, M. (2013) Subducted slabs stagnate above, penetrating through, and
726   trapped below the 660 km discontinuity. Journal of Geophysical Research, 118, 5920-5938.
727   Gale, A., Dalton, C.A., Langmuir, C.H., Su, Y. and Schilling, J-G. (2013) The mean composition
728   of ocean ridge basalts. Geochemistry, Geophysics, Geosystems, 14,
729   doi:10.1029/2012GC004334.
730   Gillon, M.A. et al. (2017) Seven temperate terrestrial planets around the nearby ultracool dwarf
731   star TRAPPIST-1. Nature, 542, 456-460.
732   Goodwin, S.P., Gribbin, J., and Hendry, M.A. (1998) The relative size of the Milky Way. The
733   Observatory, 118, 201-208.
734   Gowanlock, M.G. and Morrison, I.A. (2018) The habitability of our evolving galaxy.
735   arXiv:1082.07036v2 [astro-ph.Ep]
736   Gowanlock, M.G. (2016) Astrobiology effects of gamma-ray bursts in the Milky Way galaxy.
737   The Astrophysical Journal, 832:38, 12 pp.
738   Grand, S.P., van der Hilst, R., and Widiyantoro, S. (1997) Global seismic tomography: a
739   snapshot of convection in the Earth. GSA Today, 74, 1-6.
740   Hansen, L.N. and Warren, J.M. (2015) Qunatifying the effect of pyroxene on deformation of
741   peridotite in a natural shear zone. Journal of Geophysical Research, doi:
742   10.1002/2014JB011584.
743   Hartmann, W.K. and Davis, D.R. (1975) Satellite-sized planetesimals and lunar origin. Icarus,
744   24, 504-515.
745   Hazen, R.M., Grew, E.S., Downs, R.T., Golden, J., and Hystad, G. (2015) Mineral ecology;
746   chance and necessity in the mineral diversity of terrestrial planets. Canadian Mineralogist, 53,
747   295-324.
748   He, Y., and Wen, L. (2012) Geographic boundary of the "Pacific Anomaly" and its geometry and
749   transitional structure in the north. Journal of Geophysical Research, 117:B09308.
750   Hewins, R.H. and Herzberg, C.T. (1996) Nebular turbulence, chondrule formation, and the
751   composition of the Earth. Earth and Planetary Science Letters, 144, 1-7.
752   Hinkel, N.R., Timmes, F.X., Young, P.A., Pagano, M.D., and Turnbull, M.C. (2014) Stellar
753   abundances in the solar neighborhood: the Hypatia Catalog. The Astronomical Journal,
754   148:54 (33pp).
755   Hinkel, N.R., et al. (2016) A comparison of stellar elemental abundance techniques and
756   measurements. The Astrophysical Journal Supplement Series, 226:4, (66 p.).
757   Hinkel, N.R., and Unterborn, C.T. (2018) The star-planet connection I: using stellar composition
758   to observationally constrain planetary mineralogy for the ten closest stars, The Astrophysical
759   Journal, 853, article id. 83, 14 pp; arXiv:1709.068630v2 [astro-ph.EP] 5 Jan 2018.

23

760 Hirose, K. (2002) Phase transitions in pyrolytic mantle around 670-km depth: implications for
761   upwelling of plumes from the lower mantle. Journal of Geophysical Research, doi:
762   10.1029/2001JB000597.
763 Hirschmann, M.M., Ghiorso, M.S., and Davis, F.A. (2008) Library of experimental phase
764   relations (LEPR): a database and web portal for experimental magmatic phase equilibria data.
765   Geochemistry Geophysics Geosystems, doi:10.1029/2007GC001894.
766 Hirschmann, M.M., and Stolper, E.M. (1996) A possible role for garnet pyroxenite in the origin
767   of the "garnet signature" in MORB. Contributions to Mineralogy and Petrology, 124, 185-
768   208.
769 Hofmann, A.W. and White, W.M. (1982) Mantle plumes from ancient oceanic crust. Earth and
770   Planetary Science Letters, 57, 421-436.
771 Hyung, E., Huang, S., Petaev, M.I., and Jacobsen, S.B. (2016) Is the mantle chemically
772   stratified? Insights from sound velocity modeling and isotope evolution of an early magma
773   ocean. Earth and Planetary Science Letters, 440, 158-168.
774 Irfune, T., Shinmei, T., McCammon, C.A., Miyajima, N., Rubie, D.C., and Frost, D.J. (2010)
775   Iron partitioning and density changes of pyrolite in Earth's lower mantle. Science, 327, 193-
776   195.
777 Javoy, M., Kaminski, E., Guyot, F., Andrault, D., Sanloup, C. (2010) The chemical composition
778   of the Earth: enstatite chondrite models. Earth and Planetary Science Letters, 293, 259-268.
779 Janson, M. Bergfors, C., Goto, M., Brandner, W., and Lafrenier, D. (2010) Spatially resolved
780   spectroscopy of the exoplanet HR 8799 c. Astrophysical Journal Letters, 710, L35-L38.
781 Jordan, T.H. (1977) Lithospheric slab penetration into the lower mantle beneath the Sea of
782   Okhotsk. Journal of Geophysics, 43, 473-496.
783 Jordan, T.H., Puster, P., Glatzmaier, G.A., and Tackley, P.J. (1993) Comparisons between
784   seismic Earth structures and mantle flow models based on radial correlation-functions.
785   Science, 261, 1427-1431.
786 Kahn, A., Maclennan, J., Taylor, S.R., and Connolly, J.A.D. (2006) Are the Earth and the moon
787   compositionally alike? Inferences on lunar composition and implications for lunar origin and
788   evolution form geophysical modeling. Journal of Geophysical Research, 111,
789   doi:10.1029/2005JE002608.
790 Keil, K. (2010) Enstatite achondirte meteorites (aubrites) and the histories of their asteroidal
791   parent bodies. Chemie der Erde, 70, 295-317.
792 Kraus, A.L., Ireland, M.J., Huber, D., Mann, A.W., and Dupuy, T.J. (2016) The impact of stellar
793   multiplicity on planetary systems. I. The ruinous influence of close binary companions. The
794   Astronomical Journal, 152:8, 17 pp.
795 Krissansen-Totten, J. Garland, R., Irwin, P., and Catling, C. (2018) Detectability of biosignatures
796   in anoxic atmospheres with the James Webb Space Telescope: a TRAPPIST-1r case study.
797   The Astronomical Journal, 156:114, 13 pp.
798 Lambart, S., Baker, M.B. and Stolper, E.M. (2016) The role of pyroxenite in basalt genesis:
799   melt-PX, a melting parameterization for mantle pyroxenites between 0.9 and 5 GPa. Journal
800   of Geophysical Research, 10.1002/2015JB012762.
801 Lambart, S., Laporte, D. and Schiano, P. (2009) An experimental study of pyroxenite partial
802   melts at 1 and 1.5 GPa: implications for the major-element composition of mid-ocean ridge
803   basalts. Earth and Planetary Science Letters, 288, 335-347.
804 Le Bas, M.J. and Streckeisen, A.L. (1991) The IUGS systematics of igneous rocks. Journal of the
805   Geological Society of London, 148, 825-833.

806 Lineweaver, C.H., Fenner, Y., and Gibson, B.K. (2004) The galactic habitable zone and the age
807   distribution of complex life in the Milky Way. Science, 303, 59-62.
808 Lodders, K. (2003) Solar system abundances and condensation temperatures of the elements.
809   The Astrophysical Journal, 591, 1220-1247.
810 Lodders, K. (2010) Solar system abundances and condensation temperatures of the elements. In:
811   Principles and Perspectives of Cosmochemistry, Lecutre Notes of the Koday School on
812   'Synthesis of Elements in Stars', Astrophysics and Space Science Proceedings, Springer-
813   Verag, Berli Heidelberg, 2010, p. 379-417. ISBN 978-3-642-10351-2.
814 Lodders, K. and Fegley, B. Jr. (1997) An oxygen isotope model for the composition of Mars,
815   Icarus, 126, 373-394.
816 Lodders, K. and Fegley, B. Jr. (2018) Chemistry of the Solar System, RSCPublishing, Royal
817   Society of Chemistry, www.rsc.org., 476 p., ISBN: 978-0-85404-128-2.
818 Longhi, J. (2006) Petrogenesis of picritic mare magmas: constraints on the extent of early lunar
819   differentiation. Geochimica et Cosmochimica Acta, 70, 5919-5934.
820 Lemasle, B. et al. (2013) Galactic abundance gradients from cepheids. Astronomy and
821   Astrophysics, 558, A31, doi:10.1051/0004-6361/201322115.
822 Lopez-Corredoira, M., Prieto, C.A., Garzon, F., Wang, H., Liu, C., and Deng, L. (2018) Disk
823   stars in the Milky Way detected beyond 25 kbc from its center. Astronomy and Astrophysics,
824   612, L814 pp.
825 Luck, R.E., and Lambert, D.L. (2011) The distribution of the elements in the galactic disk. III. A
826   reconsideration of cepheids from $l = 30^o$ to 250°. The Astronomical Journal, 142:136, 16 p.p.
827 McDonough, W.F. and Sun, S.-s. (1995) The composition of the Earth. Chemical Geology, 120,
828   223-253.
829 Montelli, R., Nolet, G., Dahlen, F.A., Masters, G., Engdahl, E.R., and Hung, S-H. (2004) Finite-
830   frequency tomography reveals a variety of plumes in the mantle. Science, 303, 338-343.
831 Morgan, J.W. and Anders, E. (1979) Chemical composition of Mars. Geochimica et
832   Cosmochimica Acta, 43, 1601-1610.
833 Morgan, J.W. and Anders, E. (1980) Chemical composition of Earth, Venus and Mercury.
834   Proceedings of the National Academy of Sciences, USA, 77, 6973-6977.
835 Mulders, G.D., Pascucci, I., Apai, D., and Ciesla, F.J. (2018) The Exoplanet Population
836   Observations Simulator. I. The inner edges of planetary systems. The Astronomical Journal,
837   156, 20 pp., doi:/10.3847/1538-3881/aac5ea.
838 Murakami, M., Ohishi, Y., Hirao, N., and Hirose, K. (2012) A perovskitic lower mantle inferred
839   from high-pressure, high temperature sound velocity data. Nature, 485, 90-94.
840 Nittler, L.R., Chabot, N.L., Grove, T.L., and Peplowski, P.N. (2018) The Chemical Composition
841   of Mercury.
842 Nittler, L.R., McCoy, T.J., Clark, P.E., Murphy, M.E., Trombka, J.I., and Jaroseich, E. (2004)
843   Bulk element compositions of meteorites: a guide for interpreting remote-sensing
844   geochemical measurements of planets and asteroids. Antartctic Meteorite Research 17, 233-
845   253.
846 Palme, H. (2000) Are there chemical gradients in the inner solar system? Science Reviews, 192,
847   237-262.
848 Palme, H. and O'Neill, H.St.C. (2014) Cosmochemical estimates of mantle composition. Treatise
849   on Geochemistry, 2nd Edition. Elsevier Ltd.
850 Pottasch, S.R. (1964) A comparison of the chemical composition of the solar atmosphere with
851   meteorites. Annales de Astrophysique, 27, 163-169.

852   Prantzos, N. (2006) On the "galactic habitable zone". arXiv:astro-ph/0612316v1.

853   Putirka, K. (2005) Mantle potential temperatures at Hawaii, Iceland, and the mid-ocean ridge
854   system, as inferred from olivine phenocrysts: Evidence for thermally–driven mantle plumes.
855   Geochemistry, Geophysics, Geosystems, doi:10.1029/005GC000915

856   Putirka, K., Perfit, M., Ryerson, F.J., and Jackson, M.G. (2007) Ambient and excess mantle
857   temperatures, olivine thermometry, and active vs. passive upwelling, Chemical Geology, 241,
858   177-206.

859   Putirka, K., Ryerson, F.J., Perfit, M., and Ridley, W.I. (2011) Mineralogy and composition of the
860   oceanic mantle. Journal of Petrology, 52, 279-313.

861   Putirka, K. Tao, Y., Hari, K.R., Perfit, M., Jackson, M.G., and Arevalo Jr., R. (2018) The mantle
862   source of thermal plumes: trace and minor elements and major oxides of primitive liquids
863   (and why the olivine compositions don't matter). American Mineralogist, accepted.

864   Quarles, B., Quintana, E.V., Lopez, E., Schlieder, J.E., and Barclay, T. (2017) Plausible
865   compositions of the seven TRAPPIST-1 planets using long-term dynamical simulations.
866   arXiv:1704.02261v2 [astro-ph.EP].

867   Rackham, B.V., Apai, D., and Giampapa, MS. (2018) The transit light source effect: false
868   spectral features and incorrect densities for M-dwarf transiting planets. The Astrophysical
869   Journal, 853:122, 18 pp.

870   Ramirez, R., Gomez-Munoz, M.A., Vazquez, R., and Nunez, P.G. (2018) New numerical
871   determination of habitability in the galaxy: the SETI connection. International Journal of
872   Astrobiology, 17, 34-43.

873   Ringwood, A.E. (1966) Genesis of chondrite meteorites. Reviews of Geophysics, 4, 113-175.

874   Ringwood, A.E. (1989) Significance of the terrestrial Mg/Si ratio. Earth and Planetary Science
875   Letters, 95, 1-7.

876   Ringwood, A.E. (1991) Phase transformations and their bearing on the constitution and
877   dynamics of the mantle. Geochimica et Cosmochimica Acta, 55, 2083-2110.

878   Rubie, D.C., Frost, D.J., Mann, U., Asahara, Y., Nimmo, F., Tsuno, K., Kegler, P., Holzheid, A.,
879   and Palme, H. (2011) Heterogeneous accretion, composition and core-mantle differentiation
880   of the Earth. Earth and Planetary Science Letters, 31-42.

881   Rubie, D.C., Jacobsen, S.A., Morbidelli, A., O'Brien, D.P. Young, E.D., de Vries, J., Nimmo, F.,
882   Palme, H., and Frost, D.J. (2015) Accretion and differentiation of the terrestrial planets with
883   implications for the compositions of the early-formed Solar System bodies and accretion of
884   water. Icarus, 248, 89-108.

885   Rudnick, R.L. and Gao, S. (2003) Composition of the Continental Crust. In: Rudnick, R.K.
886   (ed.) Treatise on Geochemistry, 3, The Crust, 1–64. Oxford: Elsevier-Pergamon.

887   Salters, V.J.M. and Stracke, A. (2003) Composition of the depleted mantle. Geochemistry,
888   Geophysics, Geosystems, 5, doi:10.1029/2003GC000597.

889   Schaefer, L. and Fegley Jr., B. (2017) Redox states of initial atmosphere outgassed on rocky
890   planets and planetesimals. The Astrophysical Journal, 843:120.

891   Schuberth, B.S.A., Bunge, H.P. and Ritsema, J. (2009) Tomographic filtering of high-resolution
892   mantle circulation models: can seismic heterogeneity be explained by temperature alone?
893   Geochemistry Geophysics Geosystems, 10, doi: 10.1029/2009/GC002401.

894   Sisson, T.W., Ratajeski, K., Hankin, W.B., and Glazner, A.F. (2005) Voluminous granitic
895   magmas from common basaltic sources. Contributions to Mineralogy and Petrology, 148,
896   635-661.

897   Shields, A.L. Ballards, S., and Johnson J.A. (2016) The habitability of planets orbiting M-dwarf

898   stars. Physics Reports, 663, 1-38.
899   Sleep, N.H., and Zahnle, K. (2001) Carbon dioxide cycling and implications for climate on
900   ancient Earth. Journal of Geophysical Research 106, 1373-1399.
901   Sobolev et al. (2007) The amount of recycled crust in sources of mantle-derived melts. Science,
902   316, 412-417.
903   Steenstra, E.S., Knibbe, J.S., Rai, N., and van Westrenen, W. (2016) Constraints on core
904   formation in Vesta from metal-silicate partitioning of siderophile elements. Geochimica et
905   Cosmochimica Acta 177, 48-61.
906   Stern, R.J. (2006) Is plate tectonics needed to evolve technological species on exoplanets?
907   Geoscience Frontiers, 7 573-580.
908   Stevenson, D.J. (2003) Styles of mantle convection and their influence on planetary evolution.
909   Geodynamics, 335, 99-111.
910   Tachinami C, Senshu H, and Ida, S. (2011) Thermal evolution and lifetime of intrinsic
911   magnetic fields of super-earths in habitable zones. Astrophysical Journal, 726,
912   doi.org/10.1088/0004-637X/726/2/70.
913   Taylor, G.J. (2013) The bulk composition of Mars. Chemie der Erde, 73, 401-420.
914   Thiabaud, A., Marboeuf, U., Alibert, Y., Leya, I., and Mezger, K. (2015a) Elemental ratios in
915   stars vs. planets. Astronomy and Astrophysics, 580, A30, doi: 10.1051/0004-
916   6361/201525963.
917   Thiabaud, A., Marboeuf, U., Alibert, Y., Leya, I., and Mezger, K. (2015b) Gas composition of
918   the main volatile elements in protoplanetary discs and its implication for planet formation.
919   Astronomy and Astrophysics, 574, A138, doi: 10.1051/0004-6361/201424868.
920   Thompson, J.B. (1982) Reaction Space: An algebraic and geometric approach. In, Ferry, J.M.
921   ed., Characterization of Metamorphism Through Mineral Equilibria. Reviews in
922   Mineralogy, 10, 33-52, Mineralogical Society of America, Washington D.C.
923   Thompson, S.E. et al. (2018) Planetary candidates observed by Kepler. VIII. A fully automated
924   catalog with measured completeness and reliability based on Data Release 25. Astrophysical
925   Journal Supplement, 235:38, doi:10.3847/1538-4365/aab4f9.
926   Unterborn, C.T., Desch, S.J., Hinkel N.R., and Lorenzo, A. (2018) Inward migration o the
927   TRAPPIST-1 planets as inferred from their water-rich compositions. Nature Astronomy, 2,
928   297-302.
929   Unterborn, C.T., Hull, S.D., Stixrude, L., Teske, J.K., Johnson, J.A., and Panero, W.R. (2017)
930   Stellar chemical clues as to the rarity of exoplanetary tectonics. arXiv:1706.10282v2 [astro-
931   ph.EP] 3 Jul 2017.
932   Unterborn, C.T., Johnson, J.A. and Panero, W.R. (2015) Thorium abundances in solar twins and
933   analogs: implications for the habitability of extrasolar planetary systems. The Astrophysical
934   Journal, 806:139, 8 pp.
935   Unterborn, C.T. and Panero, W.R. (2017) The effects of Mg/Si on the exoplanetary refractory
936   oxygen budget. The Astrophysical Journal, 845:61 (9pp).
937   Vanderspek et al. (2018) TESS discovery of an ultra-short-period planet around the nearby M
938   dwarf LHS 3844. arXiv:1809.07242v1.
939   van der Hilst, R.D., and Karason, H. (2000) Compositional heterogeneity in the bottom 1000
940   kilometers of Earth's mantle: toward a hybrid convection model. Science, 283, 1885-1888.
941   Wade, J. and Wood, B.J. (2005) Core formation and the oxidation state of the Earth. Earth and
942   Planetary Science Letters, 236, 78-95.
943   Walter, M.J. (1998) Melting of garnet peridotite and the origin of komatiite and depleted

944   lithosphere. Journal of Petrology, 39, 29-60.
945 Wambsganss, J. (2016) Discovering extrasolar planets with microlensing surveys.
946   Astronomical Surveys and Big data, APS Conference Series, 505, 35-43.
947 Warren, J.M. (2016) Global varaitions in abyssal peridotite compositions. Lithos, 248-251, 193-
948   219.
949 Weller, M.B., and Lenardic, A. (2018) O the evolution of terrestrial planets: bi-stability,
950   stochastic effects, and the non-uniqueness of tectonic states. Geoscience Frontiers, 9, 91-201.
951 Wood, B.J., Kiseeva, E. and Mirolo, F.J. (2014) Accretion and core formation: the effects of
952   sulfur on metal-silicate partition coefficients. Geochimica et Cosmocimica Acta, 145, 248-
953   267.
954 Workman, R.K. and Hart, S.R. (2005) Major and trace element composition of the depleted
955   MORB mantle (DMM). Earth and Planetary Science Letters, 231, 53-72.
956 Zeng, L., Sasselov, D.D., and Jacobsen, S.B. (2016) Mass-radius relation for rocky planets based
957   on PREM. The Astrophysical Journal, 819: 127 5 pp.
958

959 **Figure Captions**
960

961 **Figure 1.** Mineral fractions calculated using Thompson (1982) (MF^{Calc}) are compared to 550
962 precisely-measured mineral fractions (MF^{Meas}) derived from 168 natural peridotite and
963 pyroxenite bulk compositions (Bodinier et al. 2008; Warren 2016); 99% of these samples contain
964 spinel and all calculated and measured mineral fractions are normalized so that Ol + Opx + Cpx
965 = 1 (e.g., for triangular plotting, as in Fig. 2). Observed modes range from 0-89% Ol, 9-44% Opx
966 and 0.3-58% Cpx. Inset equation gives results for the total regression on all 550 mineral
967 abundance estimates. Uncertainties on individual mineral grains are similar but note systematic
968 error on calculated Cpx fractions at Cpx fractions > 0.4. Also note that observed Opx fractions
969 are much less than expected for some exoplanets, which may approach nearly 100% Opx (see
970 Fig. 2).
971

972 **Figure 2.** (a) FeOt vs. SiO_2 (weight %) for exoplanet Bulk Silicate Planet (BSP) compositions,
973 calculated assuming two different models for the partitioning of Fe between core and mantle:
974 α_{Fe}= 0.263 (gray circles) and α_{Fe}= 0.311 (red circles). These are compared to estimates of bulk
975 silicate Earth (BSE), Earth's Depleted Mantle (DM), and a new BSE that assumes that Earth's
976 entire lower mantle is Plume Source Mantle (BSE with PSM; blue triangle), which is a
977 combination of 80% DM + 20% Mid-Ocean Ridge Basalt (MORB; black dot), and three
978 examples of Sol-BSP derived assuming α_{Fe}= 0.263, α_{Fe}= 0.311 and α_{Fe}= 0.494. See text for
979 explanation and Table 1 for bulk compositions. Exoplanet bulk compositions, and calculated
980 BSPs are provided in Electronic Appendix A. Also plotted are SiO_2 vs. MgO (b) and Na_2O
981 (weight %) (c) for exoplanet BSPs (EBSP) when α_{Fe}= 0.263. Panels (b) and (c) compare
982 exoplanets to terrestrial peridotites (green circles; GEOROC; http://georoc.mpch-
983 mainz.gwdg.de/georoc/) and pyroxenite bulk compositions (blue stars) from experimental studies
984 in the LEPR database (Hirschmann et al. (2008). (b) also shows terrestrial orthopyroxene (Opx)
985 compositions (LEPR); Opx has the highest SiO_2 of common ultramafic minerals, and so plots to
986 the high-SiO_2 side of Opx, e.g., with $SiO_2 > 0.56$[MgO] – 40 are plausibly quartz-saturated.
987 Exoplanets that overlap with the Opx field are possibly mono-mineralic. In (c) exoplanet BSPs
988 likely have much less Na_2O than plotted since Na is volatile—which explains why Earth has as
989 little as 25% of Sol-BSP of Na_2O (which presumes that all Na is retained). (d) shows CO_2 (wt.

28

990   %) vs. S (weight %) for EBSPs where Fe, Mg, Si, C, O, and S are all reported, and where we
991   assume that all C and S are retained during condensation and accretion; these are compared to
992   Sol-BSP, bulk Mars, BSE, DM, and CI chondrites. Earth and Mars have clearly lost most of their
993   C and S.
994
995   **Figure 3.** Exoplanet BSPs (EBSP) are plotted using the ultramafic rock diagram of Le Bas and
996   Streckeisen (1991) Major oxides of EBSPs (see Appendix A) are recast as the mineral
997   components: Olivine (Ol) = Fm_2SiO_4, Orthopyroxene (Opx) = $Fm_{1.9}Ca_{0.1}Al_{0.2}Si_{1.8}O_6$,
998   Clinopyroxene (Cpx) = $Ca_{0.6}Fm_{1.4}Al_{0.2}Si_{1.8}O_6$ and Garnet = $Fm_{2.7}Ca_{0.3}Al_2Si_3O_{12}$, where FmO =
999   FeO+MgO; the Ol-Opx-Cpx proportions are projected from garnet; mineral compositions
1000 approximate Earth's current upper mantle, at 1350^oC and reproduce mineral proportions of
1001 Workman and Hart (2005) to within 10%. Mantle mineralogy is highly sensitive to how Fe is
1002 partitioned between a silicate mantle and a metallic core, as illustrated for (a) a possibly
1003 Mercury-like or Enstatite Achondrite (EnA) case, where α_{Fe}= 0.0, (noted as "Merc-EnA"), (b)
1004 a solar bulk Earth-like scenario, with α_{Fe}= 0.263 and (c) a Mars-like case, with α_{Fe}= 0.537.
1005 Panel (b) also shows where Sol-BSP would plot if α_{Fe}= 0.494. Other bulk compositions are as
1006 in Fig. 1. In (c) we also show black arrows to indicate how mineral proportions are affected by
1007 solid solution, as the plotted high T minerals are replaced by low T, pure end-member
1008 compositions, i.e, Olivine = Fm_2SiO_4; Orthopyroxene = $Fm_2Si_2O_6$; Clinopyroxene = $CaFmSi_2O_6$;
1009 Garnet = $Fm_3Al_2Si_3O_{12}$. The net effect is to yield higher contents of garnet and olivine, and lesser
1010 amounts of Opx and Cpx. Plotted positions, especially Cpx contents, are affected by
1011 renormalization in the projection from garnet.
1012
1013 **Figure 4.** Our proposed rock classification scheme for exoplanets, based on the ratio
1014 [FeO+MgO]/SiO_2 (Table 2), for the cases of (a) α_{Fe} = 0 (Mercury- or Enstatite Achonrdite Parent
1015 Body-like), (b) α_{Fe} = 0.263 (Solar) and (c) α_{Fe} = 0.54 (Mars-like). Mws = magensiowüstite; Qtz
1016 = quartz. Other abbreviations, data sources and calculations are as in Fig. 1. The indicated rock
1017 types (Mws-normative peridotite, peridotite, pyroxenite, Qtz-normative pyroxenite) are based on
1018 our normative or standard mineral compositions, noted in Fig. 3 caption. If end-member mineral
1019 compositions are used instead, BSPs shift towards Mws-normative peridotite. Note that contrasts
1020 in the partitioning of Fe significantly affect bulk silicate planet classification.
1021
1022 **Figure 5.** In (a), (b) and (c) we compare estimates of depleted mantle (DM) and bulk silicate
1023 Earth (BSE) from Fig. 1, and bulk silicate lunar compositions from Kahn et al. (2006), to BSP
1024 estimates using carbonaceous (CC) and enstatite (EC) chondrite bulk compositions from Nittler
1025 et al. (2004) as starting compositions, assuming α_{Fe}= 0.263. Also shown are bridgmanite (Mg-
1026 perovskite, Mg-pv) and majorite compositions from Hirose (2002). In (d), (e) and (f), we
1027 compare DM, BSE and chondrite-derived BSPs using a Mars-like α_{Fe}= 0.537, with estimates of
1028 martian bulk silicate compositions as in Lodders and Fegley (1997). Panels (a)-(c) illustrate the
1029 challenge in using the Sun or chondrites as a bulk composition for Earth: while BSPs using
1030 enstatite chondrites (ECs) have CaO and Al_2O_3 contents that are too low, the most CaO- and
1031 Al_2O_3-rich BSPs from carbonaceous chondrites (CCs) overlap with Earth. But the CC-derived
1032 BSPs have SiO_2 and MgO that are too low. Estimates for BSE can have lower MgO by adding
1033 MORB, but this drives BSE estimates away from CCs with respect to CaO- and Al_2O_3. Hiding
1034 large amounts of bridgmanite and majorite might yield a Solar bulk Earth but only very specific
1035 bridgmanite compositions allow BSE to have lower SiO_2 (a) and near-Solar FeO (b).

29

1036
1037

1038
1039

Table 1. Bulk Compositions

	Sol-BSP[1a]	Sol-BSP[1b]	Sol-BSP[1c]	Sol	Continental Crust[2]	MORB[3]	DM[4]	BSE-M&S[5a]	BSE-M&S[5b]	PSM[6]	BSE (if PSM = LM)[7]	Hidden[8a] F_h=0.28	Hidden[8b] F_h=0.59	Hidden[8c] F_h=0.73
SiO_2	48.9	44.9	48.1	33.9	60.6	50.5	44.7	45.0	49.9	46.0	45.7	42.8	43.9	44.1
TiO_2	0.16	0.14	0.15	0.11	0.70	1.68	0.13	0.20	0.16	0.47	0.38	0.00	0.11	0.12
Al_2O_3	3.45	3.2	3.4	2.4	15.9	14.7	4.0	4.45	3.65	6.3	5.7	0.01	2.35	2.74
Cr_2O_3	0.80	0.73	0.78	0.55	-	0.07	0.57	0.38	0.44	0.46	0.49	1.66	0.99	0.87
FeOt	8.07	15.6	9.60	34.5	6.70	10.43	8.18	8.05	8.0	8.68	8.54	35.3	20.9	18.5
MnO	0.52	0.48	0.52	0.36	0.10	0.18	0.13	0.14	0.13	0.14	0.14	1.41	0.73	0.62
MgO	33.6	30.8	33.0	23.2	4.7	7.6	38.7	37.8	35.2	31.9	33.6	14.3	26.6	28.7
CaO	2.9	2.6	2.83	1.99	6.4	11.4	3.2	3.6	2.9	5.0	4.5	1.28	2.47	2.67
Na_2O	1.45	1.33	1.43	1.00	3.10	2.79	0.13	0.36	0.34	0.72	0.57	3.90	2.03	1.71
K_2O	-	-			1.80	0.16	0.01	0.03	0.02	0.04	0.04	-	-	-
P_2O_5	-	-			0.13	0.18	0.02	0.02	-	0.06	0.05	-	-	-
NiO	0.14	0.15	0.14	2.01	-	0.01	0.25	-	-	0.20	0.21	0.30	0.27	0.26

[1a]Bulk Silicate Planet obtained using $Fe^{BSP}/Fe^{BP} = \alpha = 0.263$, from Lodders (2010) solar composition and Earth's mantle FeO (8 wt. %); [1b]Sol-BSP obtained using $\alpha = 0.494$, from Lodders (2010) solar composition minus Fe from the core (87 wt. % Fe, 33% Earth's mass); [1c] $\alpha = 0.311$ uses Bulk Silicate Earth (McDonough and Sun 1995) and Earth's metallic core to obtain bulk Earth ; [1d]Lodders (2010) solar composition as major oxides; [2]Rudnick and Gao (2003), average continental crust. [3]Gale et al. (2013), mean MORB; [4]Workman and Hart (2005), Depleted MORB Mantle; [5a]McDonough and Sun (1995) Silicate Earth, Pyrolite Mantle 1 and [5b]CI [meteorite] model; [6]PSM = Plume Source Mantle, this study; [7]Bulk Silicate Earth (BSE), if PSM if the Lower Mantle (LM) = PSM, i.e., PSM = mantle composition between 660 km and 2890 km. [8a]Hidden mantle component if Earth (with a 33% core mass, of 87% Fe, 5% Ni and 7% Si) has solar relative abundances of Si, Mg, and Fe, etc., and the hidden components is 28% of Earth's mantle (a minimum, otherwise Al and Ti are negative), which is equivalent to depths >1,850 km, or about the bottom 1000 km of the mantle; [8c]hidden component comprises all of the mantle below 1000 km. [8c]hidden component when it comprises all the lower mantle (below 660 km).

1040
1041
1042
1043
1044
1045
1046
1047
1048
1049

31

1050 **Table 2. Classification of Exoplanetary Mantle Compositions**

Exoplanet Mantle Composition (wt. % oxides)[1]	Standard Mineralogy	% Exoplanets $\alpha_{Fe} = 0.0$	% Exoplanets $\alpha_{Fe} = 0.311$	% Exoplanets $\alpha_{Fe} = 0.537$
$\dfrac{MgO + FeOt}{SiO_2} < 0.62$	Quartz-normative pyroxenite	13.3	1.2	0.2
$0.62 < \dfrac{MgO + FeOt}{SiO_2} < 0.85$	Pyroxenite	59.8	20.6	4.2
$0.85 < \dfrac{MgO + FeOt}{SiO_2} < 1.8$	Peridotite	26.8	78.0	95.1
$\dfrac{MgO + FeOt}{SiO_2} > 1.8$	Magnesiowüstite-normative Peridotite	0.1	0.2	0.5

[1]Boundaries are drawn using limits of natural, terrestrial pyroxenite and peridotite compositions. We assume that Magnesiowüstite (Msw) saturation occurs near the upper limit of $(FeO+MgO)/SiO_2$ in Ol, and that quartz (Qtz) saturation occurs below the minimum $(FeO+MgO)/SiO_2$ of orthopyroxene. We would expect dunite mineralogies when $(FeO+MgO)/SiO_2$ is close to 1.8 and orthopyroxenite when $(FeO+MgO)/SiO_2$ is close to 0.62.
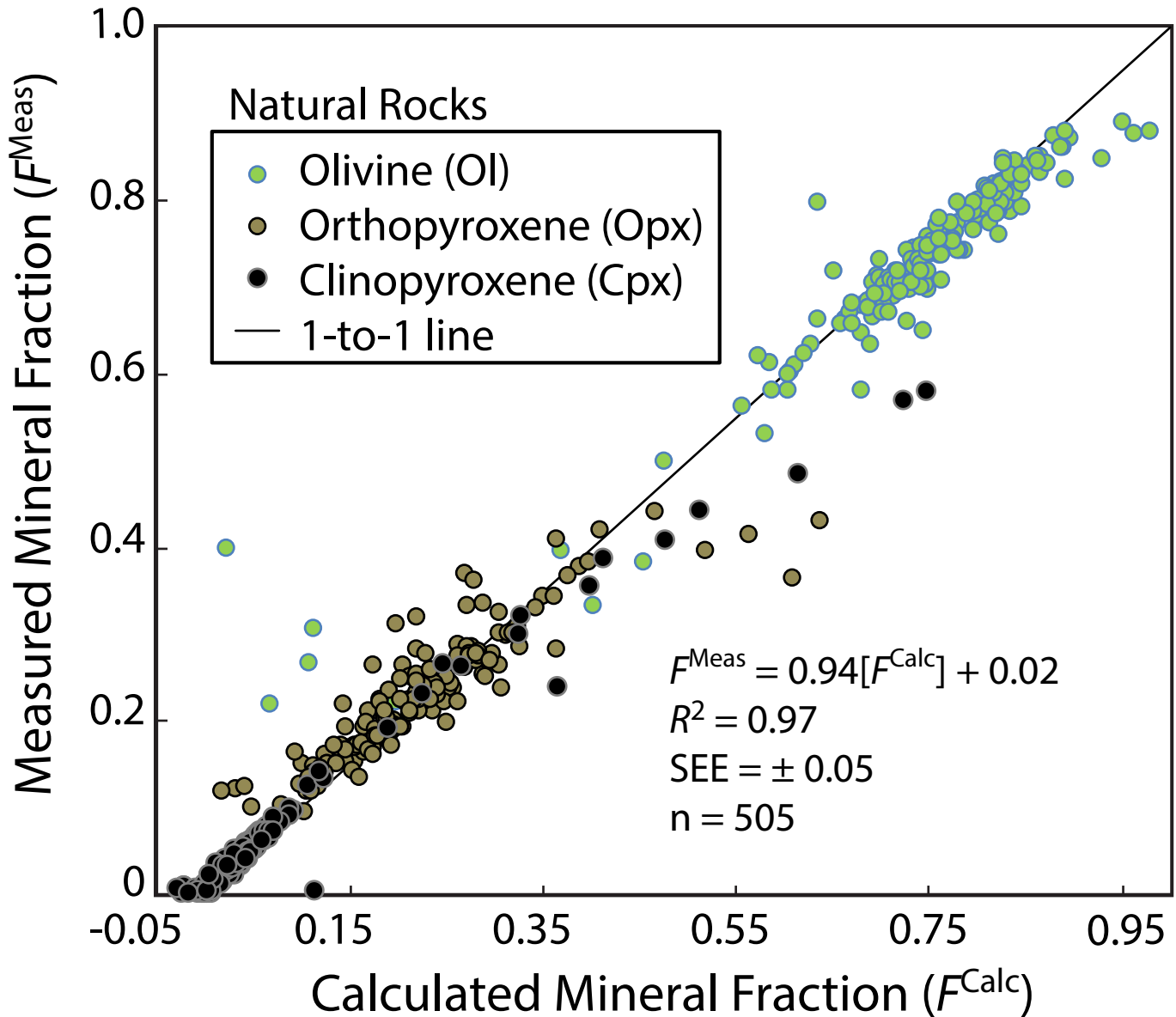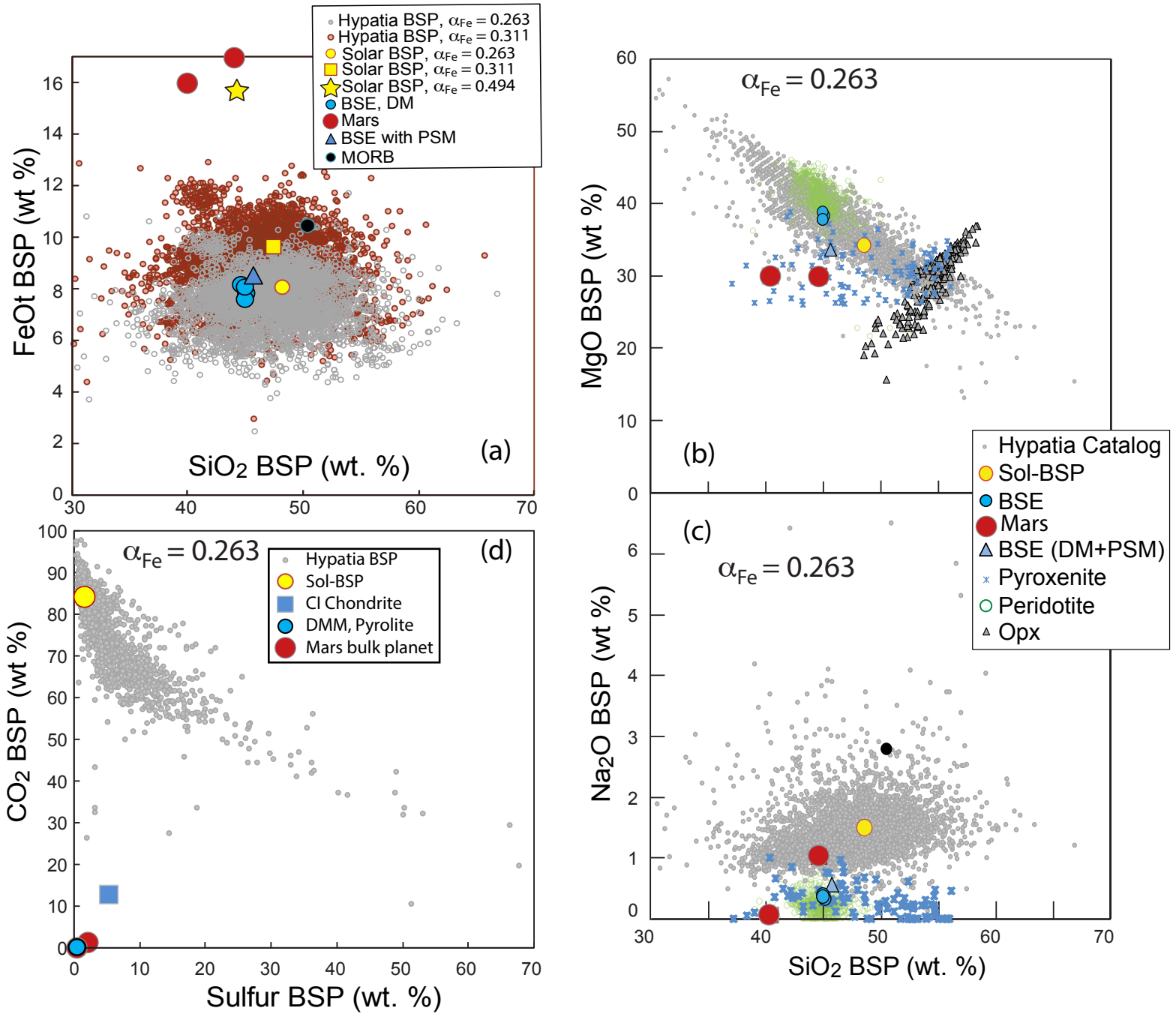
1051
1052
1053
1054
1055
1056
1057
1058
1059
1060
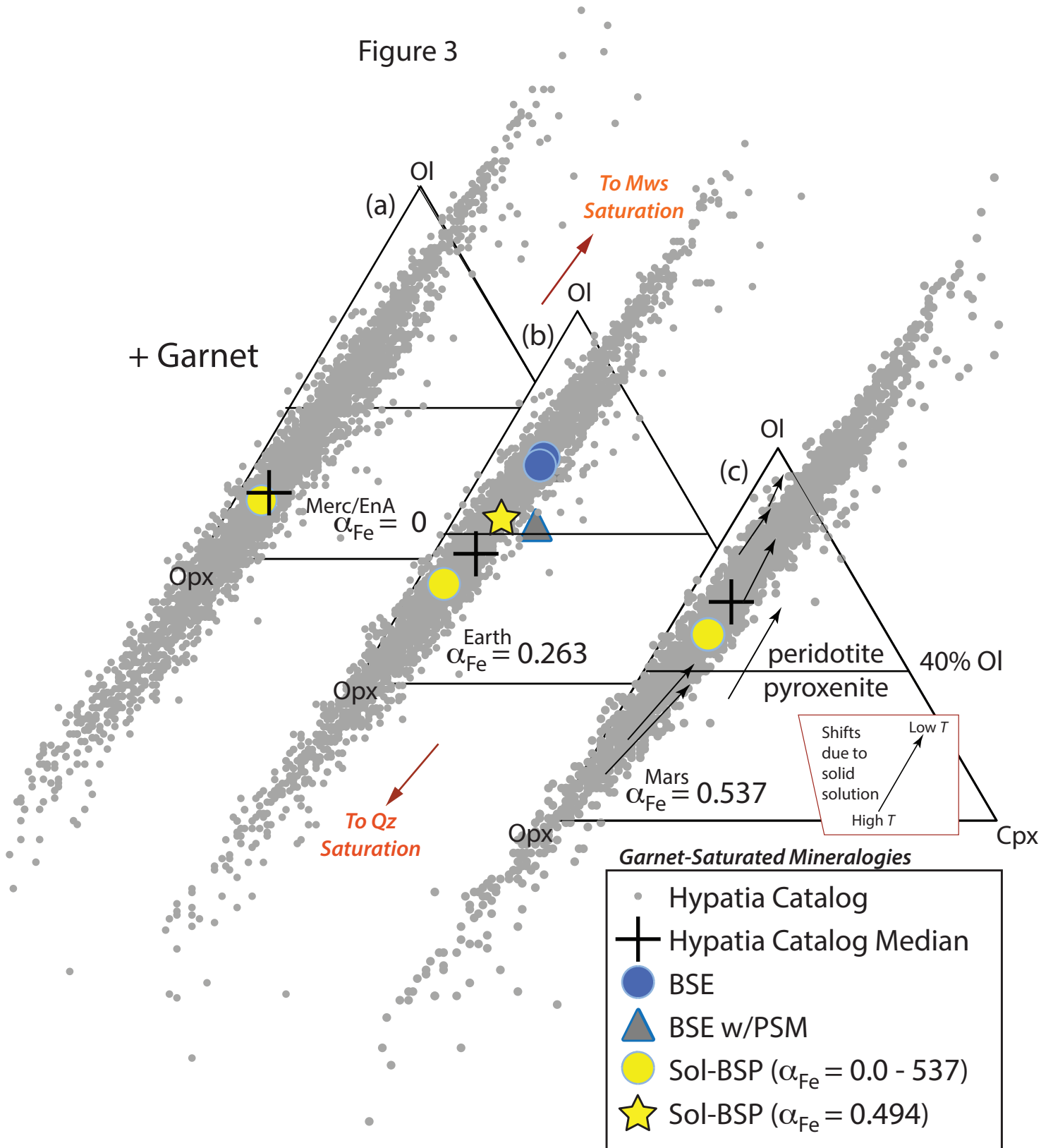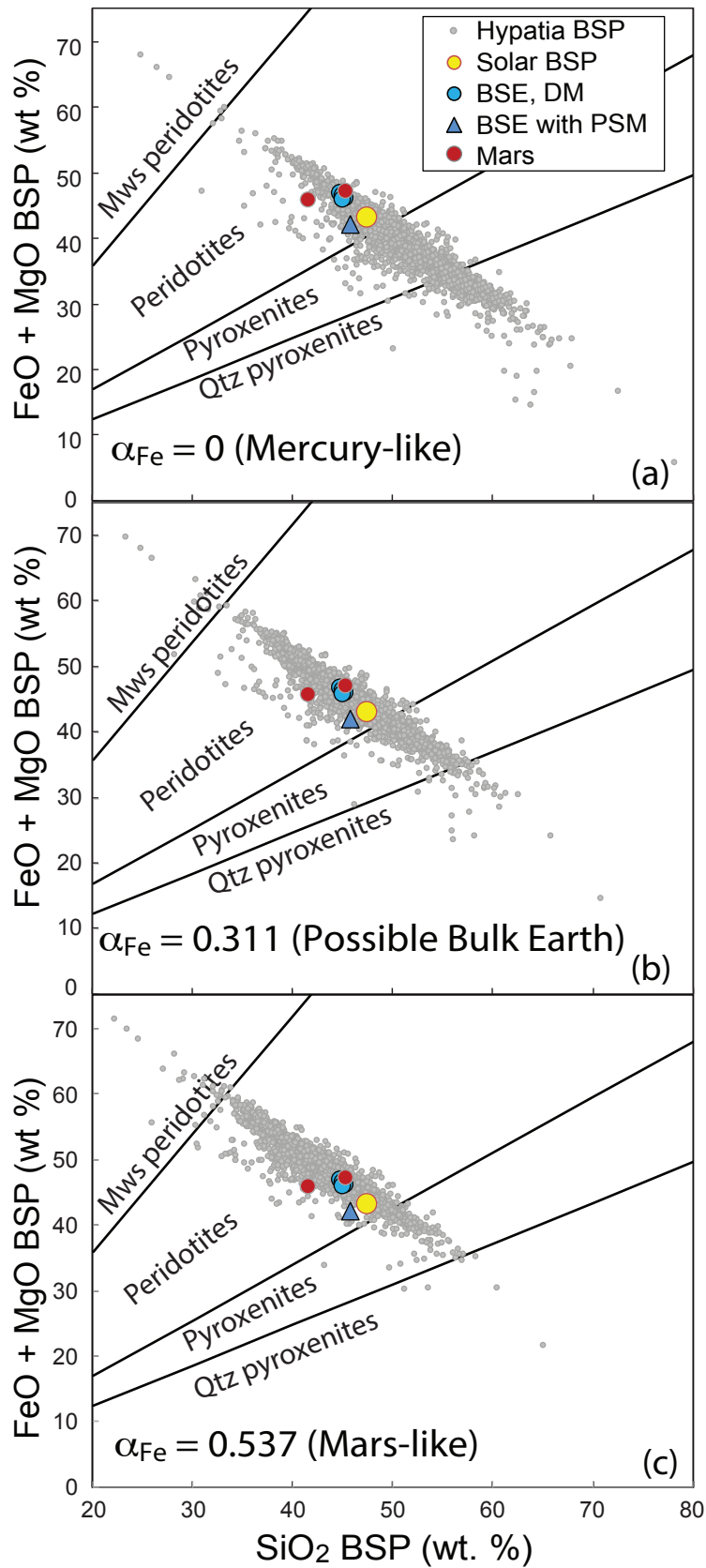1061
1062
1063
1064
1065

Figure 1

Figure 2

Figure 3

Figure 4

Figure 5